

# HYDRODYNAMIC AND MHD EQUATIONS ACROSS THE BOW SHOCK AND ALONG THE SURFACES OF PLANETARY OBSTACLES

S. M. PETRINEC\*

*Institute of Space and Astronautical Science, 3-1-1 Yoshinodai, Sagami-hara, Kanagawa 229, Japan*

C. T. RUSSELL

*Institute of Geophysics and Planetary Physics, University of California, Los Angeles, CA 90095-1567, U.S.A.*

(Received 19 June, 1996)

**Abstract.** Examinations of the magnetohydrodynamic (MHD) equations across a bow shock are presented. These equations are written in the familiar Rankine–Hugoniot set, and an exact solution to this set is given which involves the upstream magnetosonic Mach number, plasma  $\beta$ , polytropic index, and  $\theta_{B-v}$ , as a function of position along the shock surface. The asymptotic Mach cone angle of the shock surface is also given as a function of the upstream parameters, as a set of transcendental equations. The standoff position of a detached bow shock from an obstacle is also reviewed. In addition, a detailed examination of the hydrodynamic equations along the boundary of the obstacle is performed. Lastly, the MHD relations along the obstacle surface are examined, for specific orientations of the upstream interplanetary magnetic field (IMF) in relation to the upstream flow velocity vector.

## 1. Introduction

The physics of planetary bow shocks, the magnetosheath region, and obstacles such as the magnetopause have been investigated with the use of hydrodynamic and magnetohydrodynamic equations for several decades. For some circumstances, analytic solutions can be found, while under other circumstances, only numerical solutions have been determined. The purpose of this paper is to examine under what conditions analytic solutions are available, where numerical solutions are used, and where past misconceptions and misunderstandings have occurred.

The Rankine–Hugoniot relations for an isotropic plasma are used to examine the change in physical parameters (density, velocity, temperature, and magnetic field) across a planetary bow shock. As will be shown in the next section, these can be determined analytically everywhere along the bow shock surface (assuming the shock surface can be approximated as locally planar). Along the boundary of a planetary obstacle, the hydrodynamic equations (and magnetohydrodynamic equations, for a specific direction of the magnetic field) can also be solved analytically, so that the physical parameters can be known as a function of the solar wind condition. However, there are several topics for which analytic solutions are not available. The exact flow properties of plasma throughout the magnetosheath region is not known analytically. While the particle mass flux, magnetic flux, and energy must be conserved throughout the magnetosheath, this is not enough information

\* Presently at the University of Washington, Seattle, WA 98195, U.S.A.

to determine exactly where the bow shock is, or its exact shape. Even in a hydrodynamic situation with a rigid obstacle (e.g., a sphere), the bow shock position and shape has never been solved analytically and exactly (not even at the shock standoff position), though approximate solutions have been known for more than 40 years (Laitone and Pardee, 1947; Nagamatsu, 1949; Kawamura, 1950; Hida, 1953; Van Dyke and Gordon, 1959; Lomax and Inouye, 1964), and conjectures have been put forth in order to satisfy expected conditions as the Mach number approaches unity (Farris and Russell, 1994). Thus, with a magnetized plasma and a non-spherical obstacle like the magnetopause, only numerical solutions have been developed. As will be further discussed in a later section, the physics which controls the location of the magnetopause is also difficult because its shape and position are determined by means of pressure balance (in the absence of reconnection processes), and is actually self-consistently determined with the bow shock position and shape.

## 2. Across the Bow Shock

### 2.1. RANKINE–HUGONIOT RELATIONS

#### 2.1.1. *R–H Equations at Shock Subsolar Position*

As mentioned in the Introduction, the MHD equations for an ideal, adiabatic flow ( $P \propto \rho^\gamma$ ) are solvable across the bow shock. These equations are best written in the familiar form of the Rankine–Hugoniot relations. In addition, we assume here that the shock front is locally planar, and the plasma upstream and downstream of the bow shock is isotropic, such that the thermal pressure can be written as a scalar quantity, with the same value of the polytropic index ( $\gamma$ ) along and perpendicular to the magnetic field. The explicit Rankine–Hugoniot relations across the shock are then written as follows:

$$[\rho v_n] = 0, \quad (1)$$

$$\left[ \rho v_n^2 + P + \frac{B_t^2}{2\mu_0} \right] = 0, \quad (2)$$

$$\left[ \rho v_n \mathbf{v}_t - \frac{B_n}{\mu_0} \mathbf{B}_t \right] = 0, \quad (3)$$

$$\left[ \rho v_n \frac{v^2}{2} + \frac{\gamma}{\gamma - 1} v_n P + v_n \frac{B_t^2}{\mu_0} - \frac{B_n}{\mu_0} (\mathbf{v}_t \cdot \mathbf{B}_t) \right] = 0, \quad (4)$$

$$[B_n \mathbf{v}_t - v_n \mathbf{B}_t] = 0, \quad (5)$$

$$[B_n] = 0, \quad (6)$$

where square brackets denote the change in the quantity across the shock front,  $\rho$  is the plasma mass density,  $\mathbf{v}$  is the plasma bulk velocity relative to the shock,  $P$  is the thermal pressure, and  $\mathbf{B}$  is the magnetic field. The subscript  $n$  denotes the parameter component normal to the shock front, while the subscript  $t$  denotes the parameter component which is parallel to the shock front. These relations are equivalent to those used by Zhuang and Russell (1981), though the notation has been modified.

Our objective is to determine the plasma conditions and magnetic field across the shock surface, given the upstream conditions. It should be noted that this is not always the main objective of those who work with the Rankine–Hugoniot relations. For example, Lepping and Argentiero (1971) had used the relations described above to develop an iterative procedure (employing the Newton–Raphson method) to solve for the normal direction and bulk speed of the bow shock (relative to an *in-situ* spacecraft), given observations of the plasma conditions and magnetic field on either side of the shock by instruments from a single spacecraft. This work was later followed with a nonlinear least-squares fitting technique by Viñas and Scudder (1986), and these techniques were more recently improved upon by Szabo (1994) (which accounted for perturbations of the observations by plasma instabilities).

Below we rewrite Equations (7)–(13) of Zhuang and Russell (1981), which are valid for arbitrary upstream velocity and magnetic field directions incident with the shock surface. However, we use SI units here. In addition, the symbol  $\infty$  is used for values in the solar wind.

$$\Phi \equiv \rho_{\infty} v_{n\infty} = \rho v_n, \quad (7)$$

$$P = P_{\infty} + \Phi v_{n\infty} - \Phi v_n + \left( \frac{B_{t\infty}^2}{2\mu_0} \right) \\ \times \frac{(\Phi v_n)^2 - (\Phi v_{n\infty})^2 + \frac{2B_{n\infty}^2}{\mu_0} (\Phi v_{n\infty} - \Phi v_n)}{\left( \frac{B_{n\infty}^2}{\mu_0} - \Phi v_n \right)^2}, \quad (8)$$

$$\mathbf{B}_t = \mathbf{B}_{t\infty} \left( \frac{\frac{B_n^2}{\mu_0} - \Phi v_{n\infty}}{\frac{B_n^2}{\mu_0} - \Phi v_n} \right), \quad (9)$$

$$\mathbf{v}_t = \mathbf{v}_{t\infty} + \frac{B_n}{\mu_0 \Phi} (\mathbf{B}_t - \mathbf{B}_{t\infty}). \quad (10)$$

At this point we define  $X \equiv \rho_{\infty}/\rho = v_n/v_{n\infty}$  which differs by the factor  $(\rho v_n v_{n\infty})^{-1}$  from the definition of Zhuang and Russell (1981). This allows us to

rewrite the equations in terms of dimensionless variables such as Mach numbers and trigonometric functions of angles. This procedure was first used by Cairns and Grabbe (1994).

For the general problem of determining solutions of parameters everywhere across the bow shock, we must assume that at every point along the shock surface, a planar approximation can be made (i.e., the effect of shock surface curvature on the Rankine–Hugoniot equations is not considered). This approximation is expected to be valid because the ion gyroradius ( $\sim 100$  km) is more than three orders of magnitude smaller than the smallest radius of curvature of the bow shock ( $\sim 25 R_e$ , along the stagnation streamline (Farris and Russell, 1994)). We are also using a frame of reference wherein the shock surface is time stationary. This approximation must be kept in mind when comparing the solutions of the equations above with actual crossings of the bow shock with spacecraft, as the velocity of the shock front with respect to a crossing spacecraft cannot be zero. Treatment of the Rankine–Hugoniot relations for a non-time stationary shock front have been investigated by Hudson (1970), Lepping and Argentiero (1971), Viñas and Scudder (1986), Szabo (1994), and others. In addition, if the shock constantly reforms under certain conditions (e.g., when the upstream Mach number is high, and magnetic field is nearly parallel to the shock normal and upstream waves are present), as shown in many simulations (Burgess, 1989; Thomas et al., 1990; Winske et al., 1990; Onsager et al., 1991a, b; Scholer and Burgess, 1992; Scholer et al., 1993), then the above equations are expected not to be valid. Lastly, we assume from the equations above that the temperature of the plasma upstream and downstream of the bow shock is isotropic. Observationally, the plasma is rarely isotropic; particularly within the magnetosheath. The effect of temperature anisotropy has been included in the MHD equations used by Hudson (1970). The magnitude of this effect on the change in parameters across the bow shock is not known, however, and is a topic for additional study.

Before continuing on to solve Equations (7)–(10), several angles must be defined. The angle between the upstream magnetic field and velocity vectors is denoted as  $\theta_{B-v}$ . The angle between the upstream velocity vector and the shock normal (in the frame of reference which is at rest with respect to the obstacle) is defined as  $\alpha_{v-n}$ , while the angle between the upstream magnetic field vector and the shock normal is defined as  $\theta_{B-n}$ . Other angles of importance are the azimuthal angle  $\phi_{B-v}$  in the plane of the shock front, and  $\phi_{v-n}$  in the plane perpendicular to the upstream velocity vector. These angles are illustrated in Figure 1.

Using the trigonometric relations between vectors, definitions of sonic and Alfvén Mach numbers and plasma beta ( $M_s^2 \equiv \rho_\infty v_{T\infty}^2 / \gamma P_\infty$ ,  $M_A^2 \equiv \mu_0 \rho_\infty v_{T\infty}^2 / B_{T\infty}^2$ , and  $\beta = 2 / \gamma (M_A / M_s)^2$ , respectively, where the  $T$ -subscript represents the total value), and the above definition for  $X$ , Equation (4) can be rewritten (eliminating  $P$  using Equation (2), incorporating Equations (1), (3), (5), and (6), and after considerable algebra) as the following quartic equation:

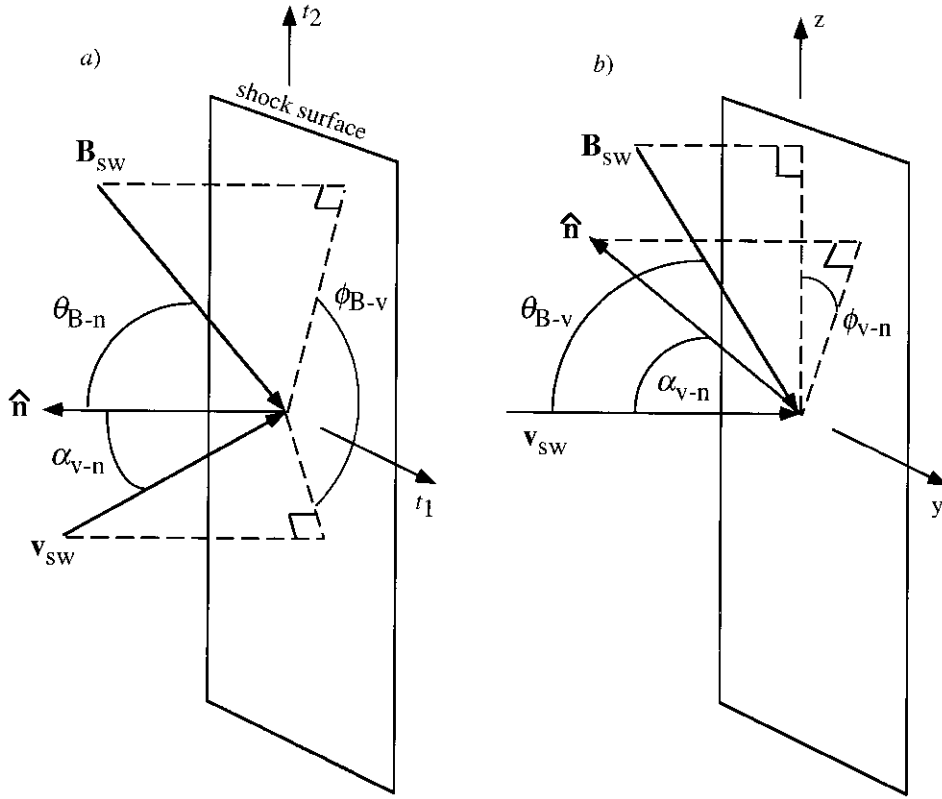


Figure 1. Schematic of the geometry used in this study. (a) Alignment with the normal to the bow shock surface. (b) Alignment with respect to the upstream solar wind velocity vector (shock surface normal to  $\mathbf{n}$  is not shown).

$$A_0 X^4 + B_0 X^3 + C_0 X^2 + D_0 X + E_0 = 0, \quad (11)$$

where

$$\begin{aligned} A_0 &= (1 + \gamma) M_A^6 \cos^6 \alpha_{v-n}, \\ B_0 &= -M_A^4 \cos^4 \alpha_{v-n} (2\gamma M_A^2 \cos^2 \alpha_{v-n} + \gamma(1 + \beta) + \cos^2 \theta_{B-n} (2 + \gamma)), \\ C_0 &= M_A^2 \cos^2 \alpha_{v-n} (M_A^4 \cos^4 \alpha_{v-n} (-1 + \gamma) + M_A^2 \cos^2 \alpha_{v-n} (\beta\gamma + 2((1 + \gamma) \\ &\quad \times \cos^2 \theta_{B-n} - (1 - \gamma))) + \cos^2 \theta_{B-n} (1 + \gamma + 2\beta\gamma)), \\ D_0 &= M_A^2 \cos^2 \alpha_{v-n} (M_A^2 \cos^2 \alpha_{v-n} (2 - \gamma - \gamma \cos^2 \theta_{B-n}) \\ &\quad - 2\gamma \cos^2 \theta_{B-n} (1 + \beta)) - \beta\gamma \cos^4 \theta_{B-n}, \\ E_0 &= \cos^2 \theta_{B-n} (M_A^2 \cos^2 \alpha_{v-n} (-1 + \gamma) + \beta\gamma \cos^2 \theta_{B-n}). \end{aligned}$$

One solution of this equation is the trivial non-shock solution,  $X = 1$ . This solution can be factored out of Equation (1), resulting in the following cubic equation:

$$A_1 X^3 + B_1 X^2 + C_1 X + D_1 = 0, \quad (12)$$

where

$$\begin{aligned} A_1 &= (1 + \gamma) M_A^6 \cos^6 \alpha_{v-n}, \\ B_1 &= M_A^4 \cos^4 \alpha_{v-n} ((1 - \gamma) M_A^2 \cos^2 \alpha_{v-n} - (\gamma + 2) \cos^2 \theta_{B-n} - \gamma(1 + \beta)), \\ C_1 &= M_A^2 \cos^2 \alpha_{v-n} ((-2 + \gamma + \gamma \cos^2 \theta_{B-n}) M_A^2 \cos^2 \alpha_{v-n} \\ &\quad + (1 + \gamma + 2\gamma\beta) \cos^2 \theta_{B-n}), \\ D_1 &= \cos^2 \theta_{B-n} ((1 - \gamma) M_A^2 \cos^2 \alpha_{v-n} - \beta\gamma \cos^2 \theta_{B-n}). \end{aligned}$$

When  $\alpha_{v-n} = 0^\circ$ , this set of equations reduces to those used by Cairns and Grabbe (1994) (which are a rewritten formulation of the set of equations derived by Zhuang and Russell (1981)). However, the set of equations above is more general and can be applied to the entire bow shock, rather than simply at the subsolar position. Away from the subsolar point the flow is not along the shock normal, though at any given point along the shock surface, one can make a frame transformation such that the upstream velocity is normal to the shock surface, and the local value of  $\alpha_{v-n}$  would be zero. This frame transformation is equivalent to a normal incidence frame (NIF) of reference, and will be discussed later in this review.

From the set of equations derived by Zhuang and Russell (1981), first-order analytic solutions to the Rankine–Hugoniot relations across the bow shock had been determined. However, though the coefficients of this cubic equation are quite complicated, the roots of this equation can, in fact, be exactly determined (contrary to the assertions of Grabbe and Cairns (1995)). The real root is most conveniently expressed as a set of nested functions, and is given below:

$$X = -\frac{t_1}{t_9 c_{\alpha 2}} - \frac{2^{1/3} t_3}{M_2^2 t_8 t_9 c_{\alpha 2}^3} + \frac{t_8}{2^{1/3} M_2^2 t_9 c_{\alpha 2}^3}, \quad (13)$$

where

$$\begin{aligned} c_{\theta 2} &= (\cos \alpha_{v-n} \cos \theta_{B-v} + \sin \alpha_{v-n} \sin \theta_{B-v} \cos \phi_{v-n})^2 \quad \{= \cos^2 \theta_{B-n}\}, \\ c_{\alpha 2} &= \cos^2 \alpha_{v-n}, \\ c_2 &= \cos^2 \theta_{B-v} \quad \{= (\cos \alpha_{v-n} \cos \theta_{B-n} + \sin \alpha_{v-n} \sin \theta_{B-n} \cos \phi_{B-v})^2\}, \\ M_2 &= M_{ms}^2 (1 + \gamma\beta/2 + ((1 + \gamma\beta/2)^2 - 2\gamma\beta c_2)^{1/2})/2 \quad \{= M_A^2\}, \end{aligned}$$

$$\begin{aligned}
 t_1 &= -\gamma(1 + \beta) + M_2 c_{\alpha 2}(1 - \gamma) - c_{\theta 2}(2 + \gamma), \\
 t_2 &= M_2 c_{\alpha 2}(-2 + \gamma) + c_{\theta 2}(1 + \gamma(1 + 2\beta + M_2 c_{\alpha 2})), \\
 t_3 &= M_2^4 c_{\alpha 2}^4(-t_1^2 + 3(1 + \gamma)t_2), \\
 t_4 &= M_2 c_{\alpha 2}(1 - \gamma) - \beta \gamma c_{\theta 2}, \\
 t_5 &= 9(1 + \gamma)M_2^6 c_{\alpha 2}^6 t_1 t_2, \\
 t_6 &= -2M_2^6 c_{\alpha 2}^6 t_1^3 - 27(1 + \gamma)^2 M_2^6 c_{\alpha 2}^6 c_{\theta 2} t_4 + t_5, \\
 t_7 &= (4t_3^3 + t_6^2)^{1/2}, \\
 t_8 &= (t_6 + t_7)^{1/3}, \\
 t_9 &= 3(1 + \gamma)M_2,
 \end{aligned}$$

where  $M_{ms}$  is the upstream magnetosonic Mach number  $M_{ms}^2 \equiv 2/(1/M_A^2 + 1/M_s^2 + ((1/M_A^2 + 1/M_s^2)^2 - 4 \cos^2 \theta_{B-v}/(M_A^2 M_s^2))^{1/2}) = 2M_A^2/(1 + \gamma\beta/2 + ((1 + \gamma\beta/2)^2 - 2\gamma\beta \cos^2 \theta_{B-v})^{1/2}) = \gamma\beta M_s^2/(1 + \gamma\beta/2 + ((1 + \gamma\beta/2)^2 - 2\gamma\beta \cos^2 \theta_{B-v})^{1/2})$ . It should be noted that this definition is in the frame of reference wherein the obstacle is at rest. In the case of the Earth, however, there is a velocity of approximately  $30 \text{ km s}^{-1}$  perpendicular to the solar wind plasma velocity due to the motion of the Earth about the Sun which must be accounted for, and will change the angle  $\theta_{B-v}$  by approximately  $4^\circ$ . Equivalent trigonometric expressions are shown in the curly brackets. In order to reduce the number of angles needed, the upstream magnetic field is defined to lie in the  $x - z$  plane, in the same manner as Zhuang and Russell (1981). The above set of equations reduces to the set derived in Russell and Petrinec (1996) for flow through the shock subsolar point ( $\alpha_{v-n} = 0^\circ$ ). Thus, the ratio of downstream to upstream parameters at any position along the bow shock surface  $\{\alpha_{v-n}, \phi_{v-n}\}$  can be determined from the solar wind inputs  $M_{ms}$ ,  $\beta$ ,  $\theta_{B-v}$ , and  $\gamma$ .

$$\rho = \rho_\infty / X, \quad (14)$$

$$B_T = B_{T\infty} \sqrt{c_{\theta 2}(1 - a^2) + a^2}, \quad (15)$$

$$P = P_\infty \left( 1 + (1 - X) \frac{2M_2}{\beta} c_{\alpha 2} + \frac{(1 - c_{\theta 2})}{\beta} (1 - a^2) \right), \quad (16)$$

$$v_T = v_{T\infty} \sqrt{1 + (X^2 - 1)c_{\alpha 2} + \frac{c_{\theta 2}(1 - c_{\theta 2})}{M_2^2 c_{\alpha 2}} (a - 1)^2 + \frac{2}{M_2} \left( c_\theta \sqrt{\frac{c_2}{c_{\alpha 2}}} - c_{\theta 2} \right) (a - 1)}, \quad (17)$$

$$P_T = P_{T\infty} \frac{2M_2 \frac{\rho}{\rho_\infty} \left( \frac{v_T}{v_{T\infty}} \right)^2 + \beta \frac{P}{P_\infty} + \left( \frac{B_T}{B_{T\infty}} \right)^2}{2M_2 + \beta + 1}, \quad (18)$$

where

$$a = \frac{c_{\theta 2} - M_2 c_{\alpha 2}}{c_{\theta 2} - X M_2 c_{\alpha 2}} \quad (19)$$

and

$$\begin{aligned} c_\theta &= \cos \alpha_{v-n} \cos \theta_{B-v} + \sin \alpha_{v-n} \sin \theta_{B-v} \cos \phi_{v-n} = \cos \theta_{B-n} \\ &= \pm (c_{\theta 2})^{1/2}, \end{aligned} \quad (20)$$

$P_T$  is the summation of the dynamic, thermal, and magnetic pressures. Although the solution provided by Equation (13) for the density ratio ( $X$ ) across the shock is complete, there can occur a singular point where values of the parameters given by Equations (14)–(18) are not physically correct. When  $\theta_{B-v} = 0^\circ$ , this occurs when the plasma  $\beta < 2/\gamma$ , and  $1 < M_2 (= M_A^2) < (1 + \gamma(1 - \beta))/(\gamma - 1)$ . Under these conditions we encounter the ‘switch-on’ shock solution at the subsolar position; i.e., the velocity and magnetic field downstream of the bow shock subsolar position acquire non-zero components parallel to the shock surface (though they remain parallel to one another downstream). When  $\gamma = \frac{5}{3}$  in the limit that  $\beta$  approaches zero, the ‘switch-on’ shock solution applies at the subsolar point for  $1 < M_{ms} < 2$ . As  $\beta$  increases the range of Mach numbers for which the ‘switch-on’ shock solution occurs shrinks and for  $\beta$  greater than 1.2 there is no ‘switch-on’ shock solution. The solution of Equation (13) above is then the ‘switch-on’ shock solution under these conditions, as it can be reduced to  $X = 1/M_2 = 1/M_A^2$  across the subsolar shock. Thus, the density ratio and velocity ratio normal to the shock surface are correctly given by Equation (14). However, it is clearly seen that at the subsolar point the downstream total magnetic field given by Equation (15) is incorrect ( $c_{\theta 2} = 1$ ). A singular point is observed in the components of the magnetic field parallel to the shock surface at the subsolar position, in comparison to positions along the shock surface infinitesimally close to the subsolar position. The ‘switch-on’ shock solution has been examined in detail by Kennel and Edmiston (1988) at the subsolar position. They found that for the ‘switch-on’ shock, the downstream speed is the intermediate shock speed. The magnitude of the tangential component of the magnetic field was shown to be determined in terms of upstream sonic and Alfvén speeds. Their solution is rewritten here in the format used above:

$$B_t = B_{T\infty} [(M_2 - 1)(1 + \gamma(1 - \beta) - M_2(\gamma - 1))]^{1/2} \equiv B_{T\infty} b'. \quad (21)$$

From this relation and Equation (13), we can proceed to determine the total magnetic field, thermal pressure, total velocity, and total pressure. Before this is done,

however, it should be noted that this formulation was designed for use at the sub-solar position (where  $\theta_{B-v} = 0^\circ$ ). However, it is important to note that even when  $\theta_{B-v} \neq 0^\circ$  but plasma  $\beta$  and the upstream magnetosonic Mach number are small enough, there is still a position on the shock surface where the upstream magnetic field is perfectly normal to the bow shock surface (provided  $\theta_{B-v} < 90^\circ - \omega$ ;  $\omega$  is the asymptotic Mach cone angle). A singular point appears at this position, and the ‘switch-on’ shock solution then applies. This is because, although the upstream velocity vector is not aligned with the upstream magnetic field vector, a simple change in the frame of reference will cause the two vectors to align, by eliminating the upstream velocity component which is parallel to the shock surface (this is the normal incidence frame (NIF) of reference). Note that this is not a global change in the frame of reference; since the parallel and perpendicular components of the solar wind velocity change along the shock surface, the NIF must be determined at each point along the shock surface. Then the specific criteria for the ‘switch-on’ solution are that  $\beta < 2/\gamma$  and  $M_2 < (1 + \gamma(1 - \beta))/(c_2(\gamma - 1))$ . Since in this study we have confined the IMF to the  $x - z$  plane, then  $\phi_{v-n} = 0^\circ$  and under these conditions, the magnetic field components at this singular point (only) can be written as:

$$\begin{aligned}
 B_n &= B_{T\infty} \cos \theta_{B-n} , \\
 B_{t1} &= 0 , \\
 B_{t2} &= B_{T\infty} (b' \cos \theta_{B-n} + \sin \theta_{B-n}) ,
 \end{aligned} \tag{22}$$

where the subscripts  $t1$  and  $t2$  are the tangential components of  $t$  along the shock surface in the  $x - y$  plane and  $x - z$  plane, respectively (and is not to be confused with the terms  $t_1$  and  $t_2$  used in the solution of Equation (13)). The total magnetic field is

$$B_T = B_{T\infty} [1 + b'^2 c_{\theta 2} + 2b' c_\theta \sqrt{(1 - c_{\theta 2})}]^{1/2} , \tag{23}$$

where  $b'$  is now generalized as

$$b' = [(M_2 c_{\alpha 2} - 1)(1 + \gamma(1 - \beta) - M_2 c_{\alpha 2}(\gamma - 1))]^{1/2} . \tag{24}$$

The thermal pressure for the downstream side at the singular position is then determined as

$$P = P_\infty \left( 1 + (1 - X) \frac{2M_2}{\beta} c_{\alpha 2} - \frac{b'}{\beta} c_\theta (b' c_\theta + 2\sqrt{1 - c_{\theta 2}}) \right) \tag{25}$$

and the total velocity is

$$v_T^2 = v_{T\infty}^2 \left( 1 + (X^2 - 1)c_{\alpha 2} + \frac{b'^2 c_{\theta 2}^2}{M_2^2 c_{\alpha 2}} + \frac{2b' c_{\theta 2}}{M_2} \sqrt{\frac{1 - c_{\alpha 2}}{c_{\alpha 2}}} \right) . \tag{26}$$

### 2.1.2. Sample Contour Plots

Along the entire shock surface comparisons of mass density and thermal pressure contours using the exact solution agree excellently (differences of less than 1%) with the contour plots of Zhuang and Russell (1981). Sample figures of the downstream to upstream ratios of mass density, thermal pressure, total velocity, total magnetic field, and total pressure across the shock surface are displayed in Figures 2–4. In these figures, the view is from the Sun, and the plots are of the polar angle  $\alpha_{v-n}$  (radial distance from the center of the plot) and azimuthal angle  $\phi_{v-n}$ . Coordinates are chosen so that the positive  $x$ -axis is directed outward, the positive  $x$ -axis points towards the top of the page ( $\phi_{v-n} = 0^\circ$ ), and the positive  $y$ -axis is directed to the right. The center of each plot represents the subsolar position. Figures 2–4 illustrate parameter ratios (calculated from Equations (14)–(18)) across the shock, for given fixed values of the upstream magnetosonic Mach number ( $M_{ms} = 5$ ), plasma beta ( $\beta = 1.2$ ), and polytropic index ( $\gamma = \frac{5}{3}$ ). The angle between the IMF and upstream velocity vector ( $\phi_{B-v}$ ) is  $0^\circ$  or  $180^\circ$  (Figure 2),  $90^\circ$  (Figure 3), and  $45^\circ$  (Figure 4), respectively. The angle  $\theta_{B-v}$  is ideally constant throughout the upstream region, and has been chosen as the independent variable for Figures 2–4. We have chosen the set  $\{M_{ms}, \beta, \theta_{B-v}, \gamma\}$  to describe the solar wind, instead of the equivalent set  $\{M_s, M_A, \theta_{B-v}, \gamma\}$ . The equivalent upstream Alfvénic and sonic Mach numbers in Figure 2 are  $M_A = M_s = 5$ ; in Figure 3,  $M_A = M_s = 7.071$ ; in Figure 4,  $M_A = M_s = 6.956$ . The angle  $\theta_{B-v}$  lies within the  $x - z$  plane, and contour levels have been chosen to lie at  $20^\circ$  intervals along the  $z$ -axis (with the exception of Figure 4, where this was not always possible). In Figure 2, the contours are circularly symmetric, as expected. In the first panel, we find that the plasma mass density ratio across the bow shock increases by nearly a factor of 4 at the subsolar point, but does not change markedly with  $\alpha_{v-n}$  until this angle becomes larger than about  $45^\circ$ . In the second panel, the thermal pressure change is quite large at the subsolar position, and decreases as  $\alpha_{v-n}$  increases. The total velocity at the subsolar point drops by nearly a factor of 4 across the bow shock, but steadily increases to match the solar wind speed. (The unity contour corresponds to the asymptotic Mach cone angle. This will be discussed in more detail below.) Although not shown, it should be noted that the change in velocity across the shock for the situation displayed in Figure 2 is such that the direction of the downstream velocity is deflected away from the shock normal (except at the subsolar position). The total magnetic field ratio is unity at the subsolar position (as it must be), but is larger at distances further from the subsolar position. However, this ratio approaches unity again far from the subsolar position. The final panel in Figure 2 displays the ratio of total pressures across the bow shock. This is not to be confused with the ratio of the pressure component normal to the bow shock, which is unity along the entire surface (as evidenced from the addition of Equations (2) and (6)). Its behavior for  $\theta_{B-v} = 0^\circ$  (or  $180^\circ$ ) is similar to that of the total magnetic field. In Figure 3, the contour values of the density and velocity ratios are similar to those in Figure 2. However, the contours are elongated in the

direction of the upstream magnetic field. The thermal pressure ratio is larger than the corresponding ratio in Figure 2, and the contours are also slightly elongated in the direction of the solar wind magnetic field vector. The total magnetic field ratio is considerably different from that of Figure 2, decreasing steadily with increasing distance from the subsolar position. The contours are also elongated, but in the direction perpendicular to the plane containing the upstream velocity and magnetic field vectors. The density ratio, the magnetic field ratio, and the inverse velocity ratio are equivalent at the subsolar point, as expected (though this is in contrast to the ideal MHD simulation results of Cairns and Lyon (1995), which shows that  $\rho/\rho_\infty < v_{T\infty}/v_T < B_T/B_{T\infty}$  on the downstream side of the subsolar bow shock for upstream  $\theta_{B-v} = 90^\circ$ ). The total pressure ratio displayed in the final panel indicates that the pressure is slightly higher along the axis containing the solar wind magnetic field than along the axis perpendicular to the upstream magnetic field.

In Figure 4, we display the same parameter ratios for  $\theta_{B-v} = 45^\circ$  and  $\phi_{B-v} = 0^\circ$  (or  $\theta_{B-v} = 135^\circ$  and  $\phi_{B-v} = 180^\circ$ ). The density contours are pulled towards the positive  $z$ -axis, with a maximum ratio at  $\alpha_{v-n} = 24^\circ$  and  $\phi_{v-n} = 0^\circ$ . The maximum thermal pressure ratio, the minimum total velocity ratio, and the minimum total pressure ratio are likewise pulled towards the positive  $z$ -axis by  $5.9^\circ$ ,  $2.4^\circ$ , and  $2.5^\circ$ , respectively. It is noted here (though not often appreciated) that the downstream bulk plasma velocity *at the subsolar shock position* is deflected from the upstream velocity direction when the upstream velocity and IMF are neither aligned with nor perpendicular to one another (the effect of the deflection of the downstream velocity caused by the IMF direction on the shape and orientation of the shock and magnetopause were investigated by Walters (1964) and Zhuang et al. (1981)). Of these parameters, it is expected that the total pressure ratio across the bow shock would best indicate a deflection of the symmetry axis of the bow shock due to the IMF. Thus, it appears that for  $\theta_{B-v} = 45^\circ$ ,  $M_{ms} = 5$ ,  $\beta = 1.2$ , and  $\gamma = \frac{5}{3}$ , there is a deflection of  $2.5^\circ$ . However, this angular value is meaningless until we relate  $\alpha_{v-n}$  to the shape of the bow shock (this is done below). In addition, this non-zero value of the angular deflection of the bow shock symmetry axis may only apply to a solid obstacle. For an obstacle such as the magnetopause, for which the shape and size is determined by the conditions of the solar wind, it is not known whether any deflection of the shock symmetry axis actually occurs (see Zhuang et al. (1981) for a comprehensive study of pressure asymmetries along the magnetopause and consequent deflection of the magnetopause symmetry axis).

The shape of the shock surface is determined by the shape of the obstacle, as noted in many earlier studies (Van Dyke and Gordon, 1959; Kellogg, 1962; Spreiter and Jones, 1963; Lomax and Inouye, 1964; Spreiter et al., 1966; Zhuang and Russell, 1981; Farris and Russell, 1994; and others). Some empirical studies fit spacecraft crossings of the bow shock to a general 2nd-order conic section in 3-dimensions (Formisano, 1979; Peredo et al., 1995). Fits to conic sections in 2-dimensions were performed by Fairfield (1971), who then went on to estimate a

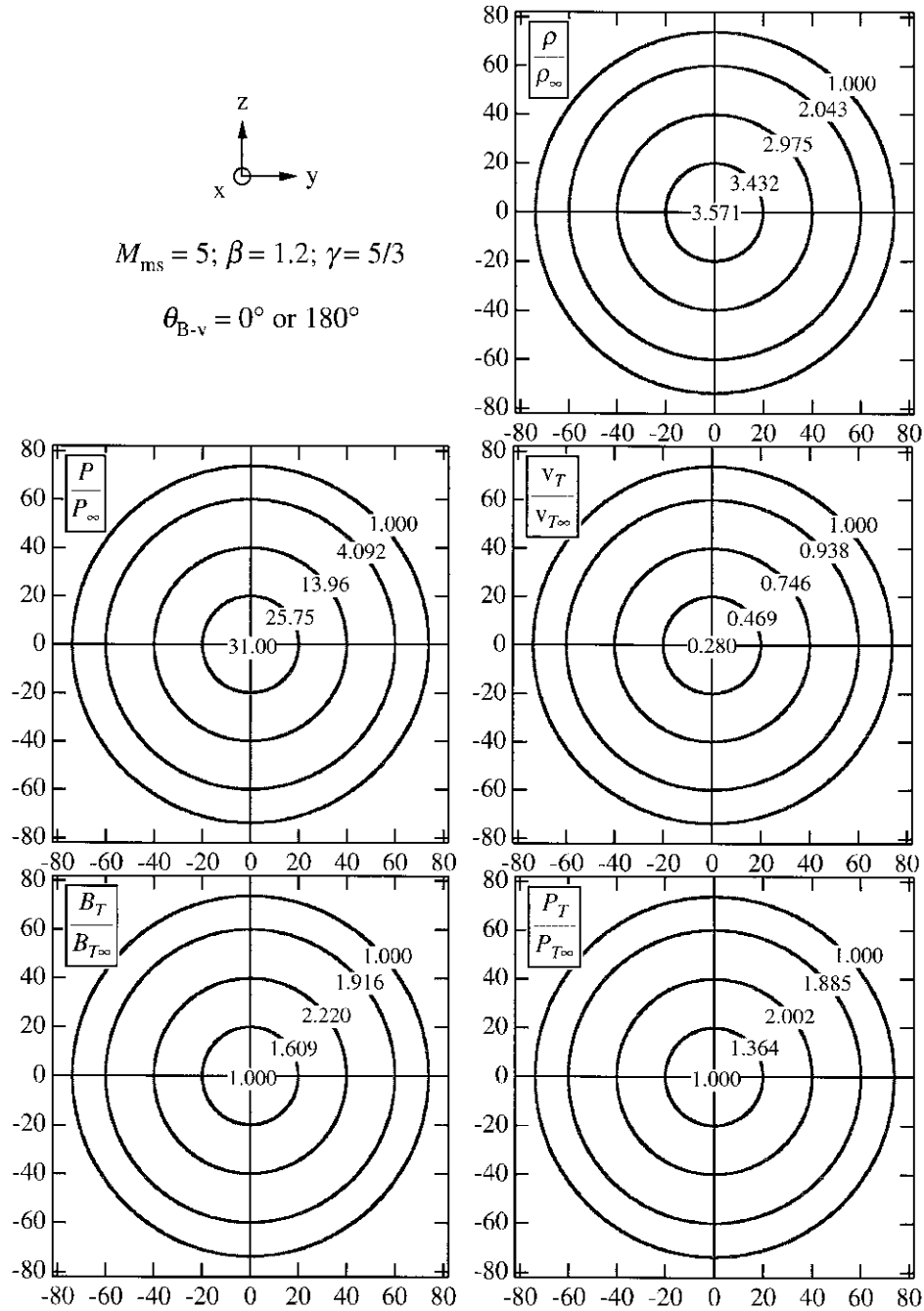


Figure 2. Contour levels representing the solutions of the Rankine-Hugoniot conditions over the shock surface, for upstream field-aligned flow. The view is from the Sun, so the upstream velocity vector is directed into the page. The magnetosonic Mach number is 5, the plasma  $\beta$  is 1.2, and the polytropic index is  $\frac{5}{3}$ . The panels include the downstream-to-upstream mass density ratio, thermal pressure, total velocity, total magnetic field, and total pressure. The axes are displayed in the upper left corner, but the plots are not in spatial coordinates. The radial distance represents  $\alpha_{v-n}$ , and the azimuthal angle is  $\phi_{v-n}$  ( $0^\circ$  along the positive  $z$ -axis).

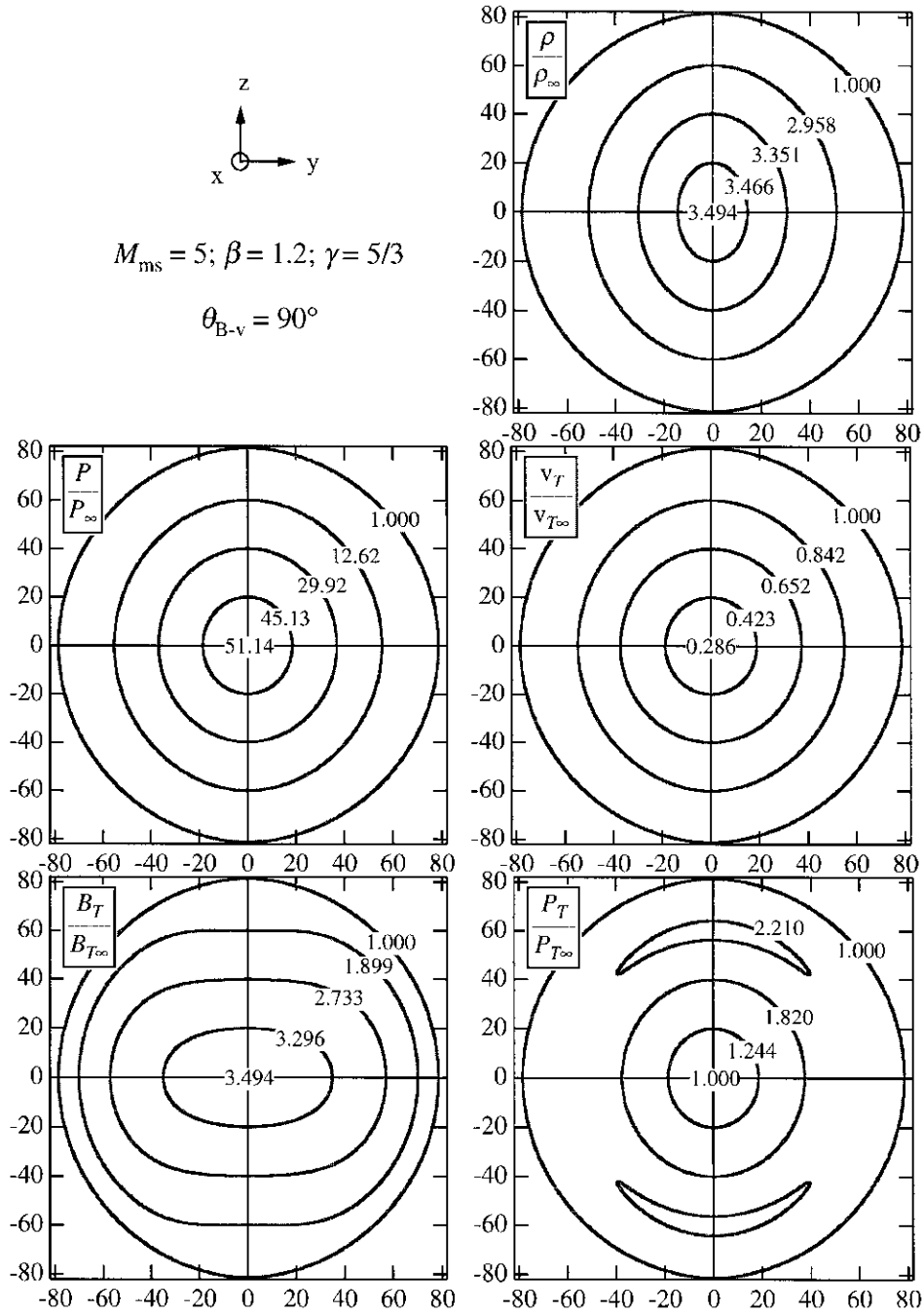


Figure 3. Same as Figure 2, but for an upstream magnetic field along the  $z$ -axis, and perpendicular to the upstream velocity vector.

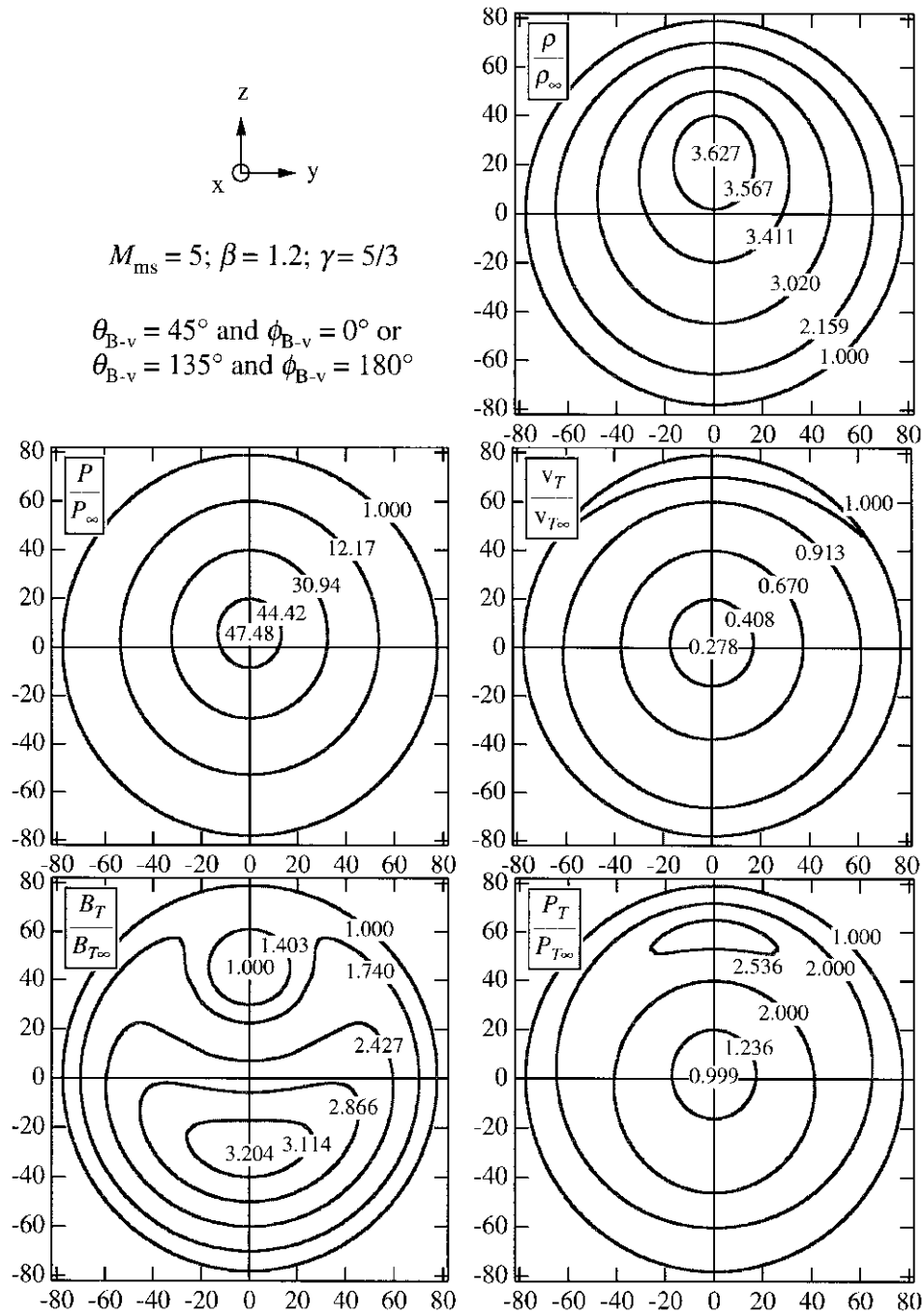


Figure 4. Same as Figure 2, but for an angle between the upstream magnetic field and upstream velocity vector of  $45^\circ$ .

simpler 2-parameter fit (the eccentricity and the subsolar distance), with the origin placed at one focus. The placement of the origin with respect to the center of the Earth can be treated as a free variable. However, Fairfield (and more recently, Farris et al., 1991) had fixed the origin at the center of the Earth, in order to better study the effects of the solar wind on the shock subsolar distance and average shape. The equation for the conic section can thus be written as:

$$r = \frac{r_0(1 + \varepsilon)}{1 + \varepsilon \cos \psi_s}, \quad (27)$$

where  $r$  is the radial distance from the Earth,  $r_0$  is the distance from the Earth to the subsolar position,  $\varepsilon$  is the eccentricity of the bow shock, and  $\psi_s$  is the angle between the solar wind vector and the normal to the bow shock surface. The relationship between  $\alpha_{v-n}$  and  $\psi_s$  can then easily be solved as

$$\cos^2 \alpha_{v-n} = c_{\alpha 2} = \frac{(\cos \psi_s + \varepsilon)^2}{\varepsilon(2 \cos \psi_s + \varepsilon) + 1}, \quad (28)$$

or, equivalently,

$$\cos \psi_s = \varepsilon(c_{\alpha 2} - 1) + \sqrt{c_{\alpha 2}(\varepsilon^2(c_{\alpha 2} - 1) + 1)}. \quad (29)$$

Using an eccentricity of 0.81 as determined empirically by Farris et al. (1991), the minimum total pressure of Figure 4 can be estimated to be at  $\psi_s = 4.5^\circ$  towards the positive  $z$ -axis.

Lastly, an interesting feature (and an important one for observers) is found in the velocity contour panel of Figure 4. Here, the total velocity ratio exceeds unity close to the asymptotic Mach contour (by at most 1.5% for these parameters). Yet the total pressure perpendicular to the surface and the total energy across the bow shock in this region are conserved. In addition, the angle of the magnetosheath velocity vector with respect to the normal is larger than the corresponding angle in the solar wind. The total magnetosheath velocity is larger than the total solar wind velocity as a consequence of the frame of reference. When viewed from the NIF of reference, the total magnetosheath velocity is less than the total solar wind velocity in the same region, with the ratio becoming equal to unity at the asymptotic Mach cone angle. In addition, the downstream magnetosonic Mach number is less than unity in this region. Thus, it should be possible for a spacecraft to observe a slight *increase* in the total velocity as it crosses from the solar wind into the magnetosheath region in a geocentric frame of reference (though this would occur very far downtail).

## 2.2. ASYMPTOTIC MACH CONE ANGLE

The outermost contour in all of the panels of Figures 2–4 is unity, corresponding to the asymptotic Mach cone angle. This is the inclination angle that the very

distant shock makes with respect to the upstream velocity vector. It is interesting to note that while the upstream magnetosonic Mach number is (ideally) a constant value for given solar wind parameters and magnetic field direction (in the frame of reference which is stationary with respect to an obstacle in the flow), the fast mode phase speed of the plasma is not spherically symmetric (as is the sound speed for an ideal gas); thus the shock wave propagates at different speeds depending upon the local orientation of the shock surface with respect to the upstream magnetic field direction. The asymptotic Mach cone angle is not a constant value, but varies with the IMF direction. In Figures 2–4 the Mach cone angle varies from  $\omega = 16.26^\circ$  ( $\alpha_{v-n} = 73.74^\circ$ , the complement of  $\omega$ ) for  $\theta_{B-v} = 0^\circ$ , to  $\omega = 8.73^\circ$  ( $\alpha_{v-n} = 81.27^\circ$ ) for  $\theta_{B-v} = 90^\circ$  (in the  $x - z$  plane), while the upstream value of  $M_{ms}$  remains constant in these figures ( $M_{ms} = 5$ ). To determine the asymptotic Mach cone angle, the appropriate expression is  $\omega = \arcsin(v_{ph}/v_{T\infty})$  (or, equivalently,  $\cos \alpha_{v-n} = v_{ph}/v_{T\infty}$ ), where

$$\frac{v_{ph}}{v_{T\infty}} = \sqrt{\frac{1}{2M_2} \left( 1 + \frac{\gamma\beta}{2} + \sqrt{\left(1 + \frac{\gamma\beta}{2}\right)^2 - 2\gamma\beta \cos^2 \theta_{B-k}} \right)}. \quad (30)$$

The angle  $\theta_{B-k}$  differs from the upstream angle  $\theta_{B-v}$ , as illustrated in Figure 5 (since the bow shock is a fast magnetosonic wave, its surface is determined from  $\theta_{B-k}$ ). In two dimensions, the angle  $\theta_{B-k} = \alpha_{v-n} \mp \theta_{B-v}$  (the sign is determined by the relative rotations (clockwise or counterclockwise) of  $\theta_{B-k}$  and  $\theta_{B-v}$  from the upstream velocity vector). As noted by Spreiter and Stahara (1985), the asymptotic Mach cone angle ( $\omega$ ) of the bow shock in the general MHD situation can only be given explicitly for special cases of  $\theta_{B-v}$  ( $0^\circ$  or  $180^\circ$ ,  $90^\circ$ , and values which result in the maximum or minimum asymptotic angle), or when there is no upstream magnetic field. In the plane containing the solar wind velocity and magnetic field vectors, the general relation for the asymptotic angle  $\alpha_{v-n}$  is:

$$2\sqrt{M_2} \cos \alpha_{v-n} = \sqrt{2 + \gamma\beta + \sqrt{(2 + \gamma\beta)^2 - 8\gamma\beta \cos^2(\alpha_{v-n} \mp \theta_{B-v})}}, \quad (31)$$

where the negative sign is chosen when  $\phi_{v-n} = 0^\circ$  (positive  $z$ -axis), and the positive sign is chosen when  $\phi_{v-n} = 180^\circ$  (negative  $z$ -axis). This equation is transcendental, so the asymptotic angle can only be found numerically. With this equation, we find that in Figure 4, the asymptotic angle  $\alpha_{v-n}$  is  $79.0^\circ$  ( $\omega = 11.0^\circ$ ) along the positive  $z$ -axis, and  $\alpha_{v-n}$  is  $78.0^\circ$  ( $\omega = 12.0^\circ$ ) along the negative  $z$ -axis. This suggests that the symmetry axis of the bow shock is deflected towards the positive  $z$ -axis for the conditions in Figure 4, though by only  $0.5^\circ$ .

The above solution for the asymptotic Mach cone angle is not complete, however, because we have only examined the  $x - z$  plane. The 3-dimensional

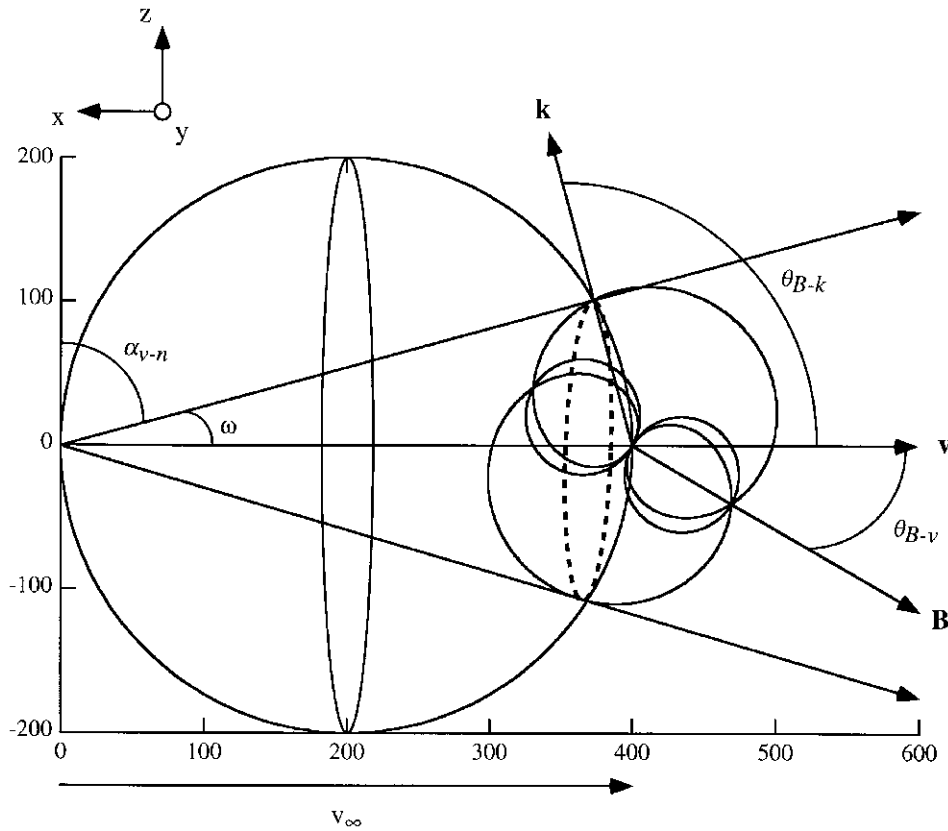


Figure 5. The geometry used to determine the asymptotic Mach cone angle ( $\omega$ ). The dotted line demarks the intersection of a velocity sphere with a Friedrichs diagram. Here,  $v_{\infty} = 400 \text{ km s}^{-1}$ ,  $M_{ms} = 5$ ,  $\beta = 1.2$ ,  $\theta_{B-v} = 30^\circ$ , and  $\gamma = \frac{5}{3}$ .  $\alpha_{v-n}$  is the complement of the Mach cone angle, and  $\phi_{v-n}$  is the azimuthal angle in the  $y - z$  plane ( $\phi_{v-n} = 0^\circ$  along the  $z$ -axis).

problem is more complicated, and is illustrated in Figure 5 (which has been adapted from similar figures in Spreiter et al. (1966) and Spreiter and Stahara (1985)). The asymptotic Mach cone angle can be determined from the intersection in velocity space of a sphere of radius  $v_{T\infty}/2$  with the usual Friedrichs diagram, which is displaced from the center of the velocity sphere by  $v_{T\infty}/2$ , and rotated by the angle  $\theta_{B-v}$ . Figure 5 is actually calculated from parameters similar to those used in Figures 2–4, except that we have used  $\theta_{B-v} = 30^\circ$ . We have also included the intermediate and slow shock solutions in the Friedrichs diagram as a visual aid, though they do not contribute to the solution we seek. The basic strategy is to find where the velocity sphere intersects the 3-dimensional Friedrichs diagram. For given values of  $\theta_{B-v}$  and  $\phi_{v-n}$  this is most easily accomplished by solving numerically the following set of transcendental equations (simply by equating the  $v_x$ ,  $v_y$ , and  $v_z$  components of the two surfaces), for  $\theta_{B-k}$ ,  $\phi_{B-k}$ , and  $\alpha_{v-n}$ .

$$\begin{aligned} \cos(2\alpha_{v-n}) + 1 &= 2 \frac{v_{ph}}{v_{T\infty}} (\cos \theta_{B-k} \cos \theta_{B-v} - \sin \theta_{B-k} \sin \theta_{B-v} \cos \phi_{B-k}) \\ &\times \sin(2\alpha_{v-n}) \sin \phi_{v-n} = 2 \frac{v_{ph}}{v_{T\infty}} \sin \theta_{B-k} \sin \phi_{B-k}, \quad (32) \end{aligned}$$

$$\begin{aligned} \sin(2\alpha_{v-n}) \cos \phi_{v-n} &= 2 \frac{v_{ph}}{v_{T\infty}} (\cos \theta_{B-k} \sin \theta_{B-v} \\ &+ \sin \theta_{B-k} \cos \theta_{B-v} \cos \phi_{B-k}), \end{aligned}$$

where  $v_{ph}/v_{T\infty}$  is given by Equation (30).

In Figure 3, we find that in the  $x - z$  plane the Mach cone angle  $\omega = 8.73^\circ$ , while in the  $y - z$  plane, it is  $11.54^\circ$ . This is true regardless of the obstacle shape (or even if the bow shock is attached or detached from the obstacle). It can be seen that as the upstream magnetosonic Mach number decreases towards unity, the Mach cone angle  $\omega$  approaches  $90^\circ$  ( $\alpha_{v-n}$  approaches  $0^\circ$ ), and the shock surface becomes planar. However, this does not tell us where the shock position is with respect to the obstacle. This topic is further addressed below.

### 2.3. THE STANDOFF DISTANCE OF THE BOW SHOCK

The standoff distance of a detached bow shock from a blunt obstacle has been of interest from the earliest studies of supersonic, aerodynamic flow (Laitone and Pardee, 1947; Nagamatsu, 1949; Kawamura, 1950; Hida, 1953; and many others). The position and shape of the bow shock is such as to allow all of the shocked fluid to be deflected and flow between the shock and the obstacle. However, the determination of the position and shape of the shock is extremely difficult to derive from the hydrodynamic or gasdynamic relations, because these relations contain no length scales. Instead, approximations and assumptions are used for the shock curvature, the form of the stream functions, the vorticity and pressure distribution in the downstream region. These parameters can also be determined from experiment, observations, or via computer simulations (the earliest studies by Van Dyke and Gordon, 1959; Lomax and Inouye, 1964; and others), which track the flow field everywhere, and iterate to a final solution, subject to physical constraints.

It was noted early on that at high Mach numbers, the sheath thickness along the stagnation streamline divided by the obstacle radius is proportional to the density ratio across the shock (Hayes, 1955). A study of experimental results and previous theories led Seiff (1962) to derive a constant of proportionality for this relation ( $\Delta/r_0 = 0.78\rho_\infty/\rho$ ). However, it was noted that scatter at low density ratios (low upstream Mach numbers) indicated that this relation may not hold under all conditions.

A Rankine–Hugoniot relation between the density ratio and upstream sonic Mach number was later used by Spreiter et al. (1966) to rewrite the relation of Seiff (1962) in terms of the upstream sonic Mach number (here written as  $M_{s\infty}$ ). Results

of wind tunnel experiments using a rigid ellipsoidal object with the approximate shape of the magnetopause also compelled Spreiter et al. to replace the coefficient 0.78 with 1.1 in the Seiff relation, resulting in the following equation:

$$\frac{D_{BS}}{D_{OB}} = 1 + 1.1 \frac{\rho_{\infty}}{\rho} = 1 + 1.1 \frac{(\gamma - 1)M_{s\infty}^2 + 2}{(\gamma + 1)M_{s\infty}^2}, \quad (33)$$

where  $D_{OB}$  is the distance from the focus of the ellipsoid to its nose, and  $D_{BS}$  is the distance from the ellipsoid focus to the shock subsolar position (it should also be noted that the average radius of curvature of the subsolar obstacle is the physically important parameter in the placement of the bow shock (see Farris and Russell, 1994, for explicit relations between the radius of curvature, obstacle eccentricity, and obstacle standoff distance). Spreiter et al. cautioned that Equation (33) should only be used for upstream sonic Mach numbers greater than 5. An extrapolation to low Mach numbers reveals that the ratio of shock to obstacle standoff distances becomes 2.1 at  $M_{s\infty} = 1$ . There is no physical basis for this value, and is contrary to expectations that the shock should retreat infinitely far from the obstacle as the Mach number approaches unity (Landau and Lifshitz, 1959).

A later study by Farris and Russell (1994) approached the shortcomings of the Spreiter et al. relation from a different perspective. They noted that a simple relation involving the downstream sonic Mach number ( $M_s^2/(1 - M_s^2)$ ) resulted in the same asymptotic value as the density ratio across the shock at high upstream sonic Mach numbers. This relation also causes the ratio of bow shock to obstacle standoff distances to retreat to infinity as the Mach number decreases towards unity:

$$\frac{D_{BS}}{D_{OB}} = 1 + 1.1 \frac{(\gamma - 1)M_{s\infty}^2 + 2}{(\gamma + 1)(M_{s\infty}^2 - 1)} = 1 + 1.1 \frac{2\rho_{\infty}/\rho}{(1 + \gamma)(1 - \rho_{\infty}/\rho)}. \quad (34)$$

This conjecture is very concise and attractive, though it has not yet been proven, and is probably not exact. The density ratio can then be determined from the solution of Equation (13) (for the subsolar shock position), in terms of plasma  $\beta$ ,  $\theta_{B-v}$  ( $= \theta_{B-n}$  at the subsolar position), and the magnetosonic Mach number. This has been done by Russell and Petrinec (1996).

Cairns and Grabbe (1994) sought to show that the upstream magnetic field can influence the position of the shock subsolar point from the obstacle standoff position, in terms of Alfvén and sonic Mach numbers, as well as  $\theta_{B-v}$  ( $= \theta_{B-n}$  at the subsolar position). However, the largest change in the shock standoff distance from the obstacle (a factor of 4) at low Alfvén Mach numbers was found to occur between  $\theta_{B-v} = 0^\circ$  and other angles. The problem in their treatment of the cubic equation at the subsolar position was that specific values of  $\theta_{B-v}$  were inserted into the cubic equation before solving it. At  $\theta_{B-v} = 0^\circ$ , there are then 3 real roots, as this procedure decouples the 2 equivalent ‘switch-on’ shock solutions from the third solution. Only the third solution was used in Cairns and Grabbe (1994), which lead to an incorrect estimate of the shock distance from the obstacle

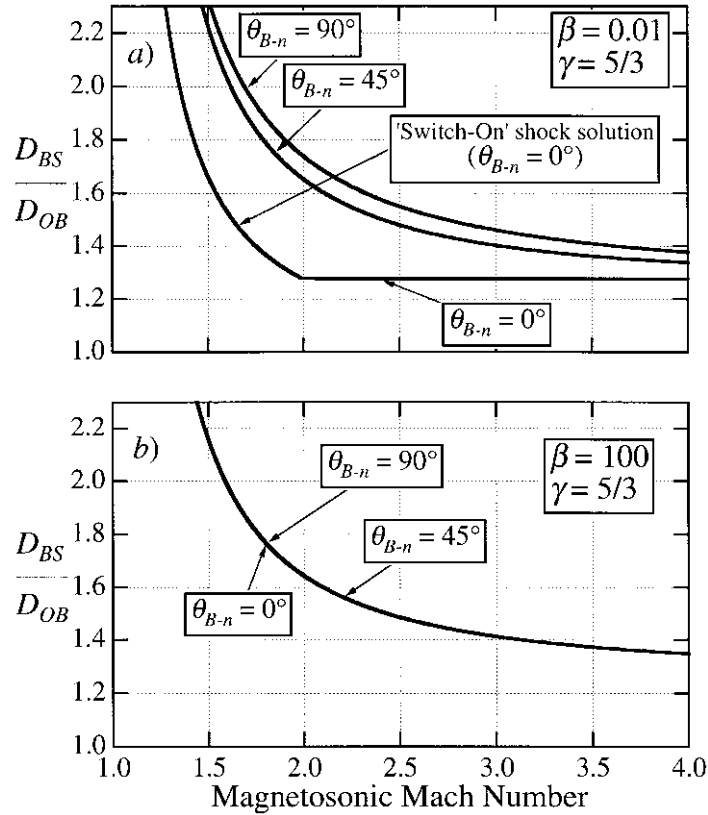


Figure 6. The ratio of distances of the bow shock and magnetopause for various values of  $\theta_{B-n}$  and  $\beta$ , as a function of magnetosonic Mach number, using the Farris and Russell (1994) conjecture. The 'switch-on' shock solution and the  $\theta_{B-n} = 0^\circ$  solution are parts of the same solution as determined from Equation (15). Adapted from Russell and Petrinec (1996).

at low Alfvén Mach numbers. This can easily be checked by noting that the density ratio does not approach unity (as it should) as the Mach number approaches unity, for  $\theta_{B-v} = 0^\circ$ . In addition, extrapolation of the Spreiter et al. solution towards Mach numbers of unity was used by Cairns and Grabbe (1994), despite the known problems. In contrast, the single solution of Russell and Petrinec (1996) (and, more generally, Equation (13) above) was solved for arbitrary  $\theta_{B-v}$  and couples the 'switch-on' shock solution to the third real solution when  $\theta_{B-v} = 0^\circ$  in the appropriate regions. Thus, this is the physical solution everywhere for the density ratio. Russell and Petrinec then used the conjecture of Farris and Russell (1994) to determine the shock subsolar position (Figure 6). Thus although it is true that the upstream magnetic field can influence the shock subsolar position, the differences are not as large as had been claimed for low Alfvén Mach numbers by Cairns and Grabbe.

However, as has been noted by Grabbe and Cairns (1995), there are several contradictory studies regarding the change in distance between the bow shock and obstacle standoff distances as a function of Alfvén Mach number. Computational solutions by Spreiter and Rizzi (1974) found that the standoff distance ratio between the bow shock and obstacle actually decreases with decreasing Alfvén Mach number (in their study,  $\theta_{B-v} = 0^\circ$ , and the lowest upstream Alfvén Mach number examined was  $M_A = 2.5$ ; thus they did not examine the behavior of the bow shock in the regime where the ‘switch-on’ shock solution applies). Recently, this claim has received observational support from the empirical study of Peredo et al. (1995). In that study, bow shock crossings obtained from (17) spacecraft were combined into a single data set, and bivariate fits performed. This result, however, is in contrast to the computational study of Cairns and Lyon (1995) (for  $\theta_{B-v} = 45^\circ$  and  $90^\circ$ ), as well as the theoretical studies of Cairns and Grabbe (1994), Grabbe and Cairns (1995), Farris and Russell (1994), and Russell and Petrinec (1996) (the latter two using magnetosonic Mach number). Part of this discrepancy may depend upon the obstacle; whether it is rigid or self-consistently solved in terms of pressure balance. Whatever the reason, continued research into this question is needed.

### 3. Pressure Balance Along the Magnetopause

#### 3.1. CASE 1: NO UPSTREAM MAGNETIC FIELD

The magnetopause can be described simply as a boundary at which the pressure of the magnetosheath (which is related to the pressure of the solar wind) is balanced by the pressure produced by the Earth’s intrinsic magnetic field (and a very small contribution from the thermal pressure of the plasma interior to the magnetosphere). One important point to consider is that in equilibrium, total pressure (the summation of dynamic, thermal, and magnetic pressures) is balanced across the subsolar bow shock, and total pressure is balanced across the magnetopause. However, along the stagnation streamline the total pressure at the magnetopause is *not* equal to the total pressure just downstream of the bow shock. The reason for this is that the flow characteristics change within the magnetosheath so as to satisfy the MHD relations (in particular, Bernoulli’s Equation), and deflect the plasma flow around the obstacle.

It is of interest to examine the parameters of plasma flow along the outer surface of the magnetopause, in terms of the solar wind parameters. In general, analytic formulations of the plasma flow parameters in the magnetosheath region are not known. However, the stagnation streamline lies closest to the magnetopause, and much can be understood from consideration of this single streamline.

We begin this examination by first considering a simple hydrodynamic flow, so that no external magnetic field exists. Then the Rankine–Hugoniot relations across the bow shock at the subsolar point can be simply written as

$$P = P_\infty \left( 1 + \frac{2\gamma}{\gamma + 1} (M_{s\infty}^2 - 1) \right), \quad (35)$$

$$M_s^2 = \frac{1 + M_{s\infty}^2(\gamma - 1)/2}{\gamma M_{s\infty}^2 - (\gamma - 1)/2}, \quad (36)$$

$$\rho = \rho_\infty \frac{(\gamma + 1)M_{s\infty}^2}{(\gamma - 1)M_{s\infty}^2 + 2}, \quad (37)$$

$$v_T = v_{T\infty} \left( \frac{(\gamma - 1)M_{s\infty}^2 + 2}{(\gamma + 1)M_{s\infty}^2} \right), \quad (38)$$

where  $M_{s\infty}$  is the solar wind sonic Mach number, and  $M_s$  is the Mach number on the downstream side of the bow shock (cf., Landau and Lifshitz, 1959). Using Bernoulli's equation ( $(v_T^2/2) + (\gamma/(\gamma - 1))(P/\rho) = \text{const.}_1$ ) and the condition of adiabatic flow ( $P\rho^{-\gamma} = \text{const.}_2$ ) between the downstream side of the bow shock and the obstacle stagnation position, the stagnation thermal pressure can be determined as

$$P_{st} = P \left( 1 + \frac{\gamma - 1}{2} M_s^2 \right)^{\gamma/(\gamma-1)}. \quad (39)$$

By substituting Equation (35) into Equation (39), and using the Mach number relation defined by Equation (36), we arrive at the following relation between the stagnation thermal pressure and the solar wind thermal pressure:

$$P_{st} = P_\infty \left( \frac{(\gamma + 1)^{\gamma+1} (M_{s\infty}^2/2)^\gamma}{2\gamma M_{s\infty}^2 - (\gamma - 1)} \right)^{1/(\gamma-1)}, \quad (40)$$

or, using the definition of the upstream sonic Mach number,

$$P_{st} = \rho_\infty v_{T\infty}^2 \frac{1}{\gamma M_{s\infty}^2} \left( \frac{(\gamma + 1)^{\gamma+1} (M_{s\infty}^2/2)^\gamma}{2\gamma M_{s\infty}^2 - (\gamma - 1)} \right)^{1/(\gamma-1)} = k \rho_\infty v_{T\infty}^2 \quad (41)$$

(cf., Landau and Lifshitz, 1959; Spreiter *et al.*, 1966; Zhang *et al.*, 1991). The value of  $k$  approaches 0.881 as the upstream sonic Mach number approaches infinity, for a polytropic index ( $\gamma$ ) of  $\frac{5}{3}$ .

The thermal pressure along the obstacle surface is then determined with the Newtonian approximation:

$$P_\psi|_{OB} = k \rho_\infty v_{T\infty}^2 \cos^2 \psi + Q = P_{st} \cos^2 \psi + Q, \quad (42)$$

where the symbol  $Q$  is used to indicate the uncertainty involving the Newtonian approximation. The density along the surface is determined with the use of the adiabatic condition:

Table I

Explicit expressions for the thermal pressure, mass density, and total velocity along the obstacle surface, for  $\gamma = \frac{5}{3}$  and  $P_\psi|_{OB} = P_{st} \cos^2 \psi$

Parameter	Pressure relation $\rightarrow P_\psi _{OB} = P_{st} \cos^2 \psi$
$P_\psi _{OB} =$	$P_\infty \frac{4^4}{3^{5/2}} \frac{M_{s\infty}^5}{(5M_{s\infty}^2 - 1)^{3/2}} \cos^2 \psi$
$\rho_\psi _{OB} =$	$\rho_\infty \frac{4^4}{3^{3/2}} \frac{M_{s\infty}^5}{(M_{s\infty}^2 + 3)(5M_{s\infty}^2 - 1)^{3/2}} \cos^{6/5} \psi$
$v_\psi _{OB} =$	$v_{T\infty} \sqrt{\frac{(M_{s\infty}^2 + 3)}{M_{s\infty}^2} (1 - \cos^{4/5} \psi)}$

Table II

Same as Table I, except  $P_\psi|_{OB} = P_{st} \cos^2 \psi + P_\infty$

Parameter	Pressure relation $\rightarrow P_\psi _{OB} = P_{st} \cos^2 \psi + P_\infty$
$P_\psi _{OB} =$	$P_\infty \left[ \frac{4^4}{3^{5/2}} \frac{M_{s\infty}^5}{(5M_{s\infty}^2 - 1)^{3/2}} \cos^2 \psi + 1 \right]$
$\rho_\psi _{OB} =$	$\rho_\infty \frac{4^{8/5} M_{s\infty}^2}{(M_{s\infty}^2 + 3)(5M_{s\infty}^2 - 1)^{3/2}} \left[ \frac{4^4}{3^{5/2}} M_{s\infty}^5 \cos^2 \psi + (5M_{s\infty}^2 - 1)^{3/2} \right]^{3/5}$
$v_\psi _{OB} =$	$v_{T\infty} \sqrt{\frac{(M_{s\infty}^2 + 3)}{M_{s\infty}^2} \left( 1 - \left( \cos^2 \psi + \frac{3^{5/2} (5M_{s\infty}^2 - 1)^{3/2}}{4^4 M_{s\infty}^5} \right)^{2/5} \right)}$

$$\rho_\psi|_{OB} = \rho \left( \frac{P_\psi|_{OB}}{P} \right)^{1/\gamma} \tag{43}$$

and Bernoulli’s equation can be utilized to determine the velocity along the surface:

$$v_\psi^2|_{OB} = v_T^2 \left( 1 + \frac{2}{(\gamma - 1)M_s^2} \left[ 1 - \left( \frac{P}{P_\psi|_{OB}} \right)^{(1-\gamma)/\gamma} \right] \right) \tag{44}$$

In Equations (42)–(44),  $\psi$  defines the angle between the upstream flow velocity vector and the normal to the obstacle. Below, we investigate this problem more closely, using different functions in place of  $Q$ . Tables I–III give simplified but explicit expressions for the thermal pressure, density, and velocity along the boundary with  $\gamma = \frac{5}{3}$ , for the pressure balance relations given below.

3.1.1.  $P_\psi|_{OB} = P_{st} \cos^2 \psi = k\rho_\infty v_{T\infty}^2 \cos^2 \psi; Q = 0$

This formulation provides a simple and useful approximation for the pressure balance at the dayside magnetopause, for high Mach numbers.  $P_\psi|_{OB}$  is the thermal

Table III  
Same as Table I, except  $P_\psi|_{OB} = P_{st} \cos^2 \psi + P_\infty \sin^2 \psi$

Parameter	Pressure relation $\rightarrow P_\psi _{OB} = P_{st} \cos^2 \psi + P_\infty \sin^2 \psi$
$P_\psi _{OB} =$	$P_\infty \left[ \frac{4^4}{3^{5/2}} \frac{M_{s\infty}^5}{(5M_{s\infty}^2 - 1)^{3/2}} \cos^2 \psi + \sin^2 \psi \right]$
$\rho_\psi _{OB} =$	$\rho_\infty \frac{4^{8/5} M_{s\infty}^2}{(M_{s\infty}^2 + 3)(5M_{s\infty}^2 - 1)^{3/2}} \left[ \frac{4^4}{3^{5/2}} M_{s\infty}^5 \cos^2 \psi + (5M_{s\infty}^2 - 1)^{3/2} \sin^2 \psi \right]^{3/5}$
$v_\psi _{OB} =$	$v_{T\infty} \sqrt{\frac{(M_{s\infty}^2 + 3)}{M_{s\infty}^2} \left( 1 - \left( \cos^2 \psi + \frac{3^{5/2} (5M_{s\infty}^2 - 1)^{3/2}}{4^4} \frac{\sin^2 \psi}{M_{s\infty}^5} \right)^{2/5} \right)}$

pressure along the outer surface of the boundary which, for a surface like the magnetopause which is defined by pressure balance, is equivalent to the summation of pressures interior to the magnetosphere (often stated as  $B_{msphere}^2/2\mu_0$ ). This relation has been used by numerous authors, using various values for  $k$  (Spitzer (1956), Dungey (1958), Zhigulev and Romishevskii (1960), Beard (1960), Hurley (1961), Mead and Beard (1964), Mead (1966), Olson (1969), and Parks (1991) used a value of  $k = 2$ , while Ferraro (1952), Piddington (1960), Dungey (1961), Parker (1961), Spreiter and Briggs (1961, 1962) used  $k = 1$ . A proper understanding of the value of  $k$  was first provided by Spreiter et al. (1966), and this value was used by later authors such as Unti and Atkinson (1968), Spreiter and Rizzi (1974), Sibeck et al. (1991), Zhang et al. (1991), and Sibeck (1995)). The best value for  $k$  takes into account the inelastic interaction of the solar wind. It does not bounce back toward the Sun. Thus  $k$  is unity adjusted downward by about 12% to account for the divergence of the streamlines around the obstacle. Nevertheless there is a problem with this relation. Specifically, this formulation breaks down as  $\psi$  approaches  $90^\circ$  because the exterior pressure as determined by this relation approaches zero. If this were true, then either the magnetotail radius would never reach an asymptotic value far downtail, or the total pressure interior to the magnetopause would decrease to zero far downtail. This is contrary, however, to observations. In addition, the magnetosheath velocity along the magnetopause surface as determined from Equation (30) exceeds the solar wind velocity as  $\psi$  approaches  $90^\circ$ , as illustrated in Figures 7 and 8 for a polytropic index of  $\frac{5}{3}$  and upstream sonic Mach numbers of 5 and 1.1, respectively. In a purely hydrodynamic flow this cannot happen (Spreiter et al., 1966), because there is no source for the additional kinetic energy. This clearly illustrates that this relation is a poor approximation far downtail.

### 3.1.2. $P_\psi|_{OB} = P_{st} \cos^2 \psi + P_\infty; Q = P_\infty$

This formulation has been used by several authors (Spreiter and Alksne, 1968, 1969; Coroniti and Kennel, 1972; Howe and Binsack, 1972; Sibeck et al., 1985;

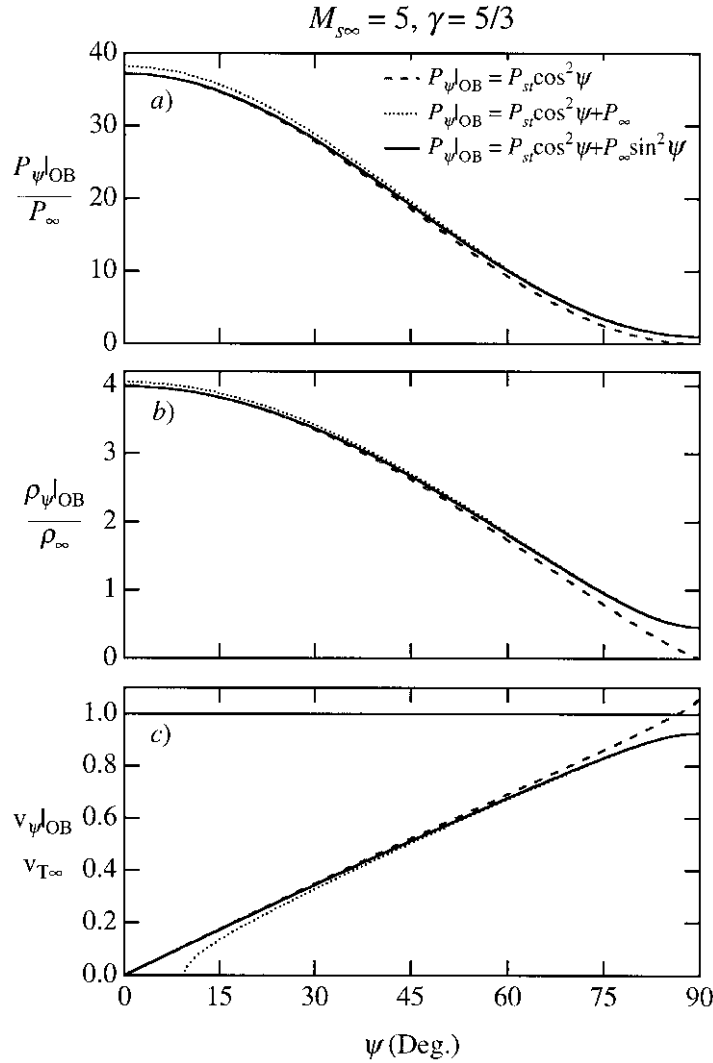


Figure 7. Hydrodynamic parameters along the magnetopause, for  $M_{s\infty} = 5$  and  $\gamma = \frac{5}{3}$ .  $\psi = 0^\circ$  corresponds to the subsolar position, while  $\psi = 90^\circ$  corresponds to the position of the boundary surface which is parallel to the upstream velocity vector. (a) Thermal pressure ratio. (b) Mass density ratio. (c) Total velocity ratio.

Slavin et al., 1985; Petrinec and Russell, 1993, 1996; Zhang et al., 1994, 1995; Spreiter and Stahara, 1995), and provides reasonably accurate solutions for large upstream Mach numbers. Usually, the solar wind magnetic field pressure is also added to the right-hand side, and  $P_\infty$  is replaced with  $P_{\text{static}}$ . This equation, however, is again only an approximation. The addition of these pressure components of the solar wind is to provide a finite external pressure to the magnetosphere as  $\psi$  approaches  $90^\circ$ . Here we consider the hydrodynamic case only, with no solar wind

magnetic field. Figures 7 and 8 also illustrate the normalized thermal pressure, ion density, and velocity along the magnetopause surface. It can be seen that while the magnetosheath thermal pressure and density are now non-zero at  $\psi = 90^\circ$ , these values are also larger at the stagnation point than the previous relation. In particular the thermal pressure does not agree with that derived in Equation (41), indicating that this relation is incorrect near the stagnation region. This point is even more clearly shown with the consideration of the velocity relation near the obstacle. While the velocity remains less than the solar wind velocity far downtail, the velocity is imaginary in the subsolar region (and over much of the dayside magnetosphere for  $M_{s\infty} = 1.1$  (Figure 8)).

$$3.1.3. \quad P_\psi|_{OB} = P_{st} \cos^2 \psi + P_\infty \sin^2 \psi; \quad Q = P_\infty \sin^2 \psi$$

This is the simplest formulation which satisfies both the demands of hydrodynamic flow at the stagnation position, as well as the demands far downtail (see Figures 7 and 8). This appears to be the only solution that satisfies all of the above conditions and for which the parameters vary monotonically from the subsolar region to the distant downtail region. Thus it should be used at a minimum when there are boundaries which are defined by a balance of pressure. This relation has in fact been used in earlier aerodynamic studies; e.g., Linnell (1958) (hypersonic flow around a sphere) and Daskin and Feldman (1958) (hypersonic flow for a sail (a surface which is also defined by pressure balance)), but not in magnetospheric applications.

One aspect not discussed in the above treatment of plasma flow near the magnetopause is the concept of centrifugal force. This force was first considered in detail by Busemann (1933), and has since come to be known as the Newton–Busemann approximation. The conjecture is that as the flow is forced around a curved obstacle, the fluid experiences a centrifugal force. The Newton–Busemann ‘approximation’ suggests that there is a substantial *decrease* to the pressure of the fluid upon the obstacle, and implies the total pressure exterior to the obstacle becomes negative before  $\psi$  even reaches  $90^\circ$ . This decrease has been considered in the past to not be valid for hydrodynamic flow around a solid obstacle for several reasons (cf., Seiff, 1962), not the least of which is that the differences are much larger than are observed experimentally. Nevertheless, the Newton–Busemann approximation has been used in studies of magnetospheric physics (Freeman et al., 1995). Freeman et al. (1995) postulate that the flow can detach from the magnetopause surface as a shock wave. They further theorize that this shock layer is thickened, though it has never been modeled. Centrifugal acceleration effects near the magnetopause were also used by Zwan and Wolf (1976) for the case of a perpendicular upstream magnetic field. It is unclear, especially for an obstacle whose size and shape are determined by pressure balance, how any centrifugal acceleration would affect the flow. More thorough theoretical studies of the pressure across the magnetopause, and throughout the magnetosheath are needed.

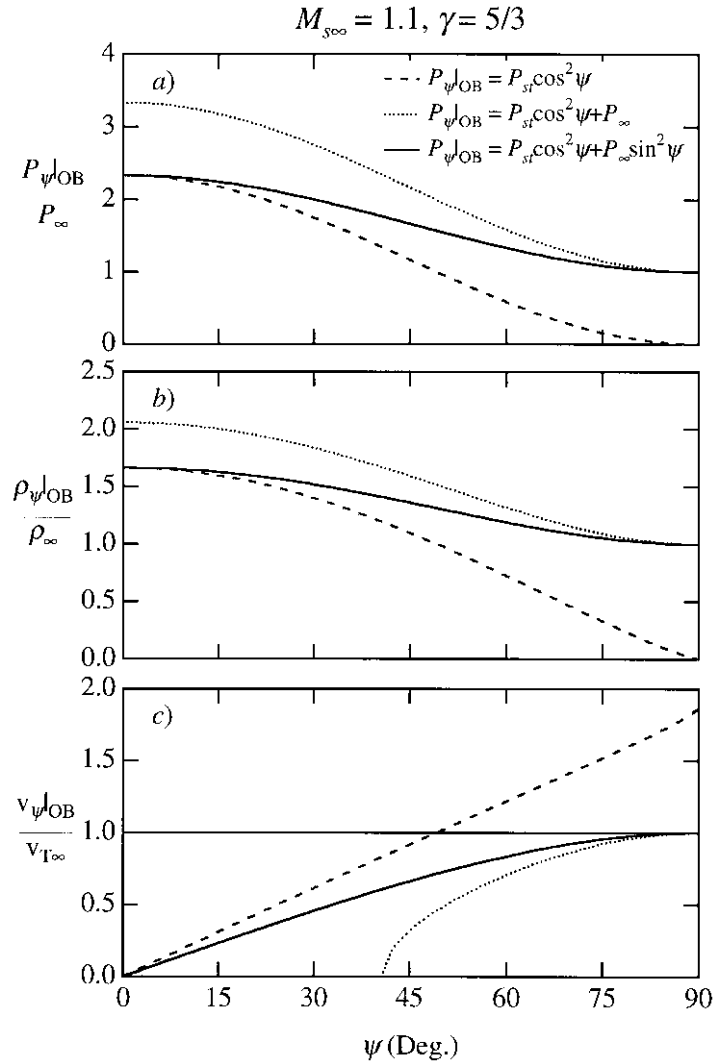


Figure 8. Same as Figure 7, but for  $M_{s\infty} = 1.1$ .

3.2. WITH MAGNETIC FIELD ( $\theta_{B-v} = 0^\circ$  OR  $180^\circ$ )

We now examine the effect of the inclusion of an upstream magnetic field vector parallel to the upstream velocity vector. It can be shown that Equations (35)–(38) remain unchanged (as long as the shock is not a ‘switch-on’ shock, which will be discussed further below). In the case of field-aligned flow, there can be no energy transfer between the magnetic and kinetic energies of the plasma, and the equations are decoupled. It can also be shown that in this situation, Bernoulli’s equation remains the same. Thus, the parameters along the obstacle (the thermal

pressure, density, and velocity) are described exactly by Equations (42)–(44), and are independent of the magnetic field. Since the magnetic field is everywhere parallel to the velocity vector (because the tangential electric field must be zero on both sides of the bow shock, given implicitly by Equation (5) above), and because both the magnetic field and the mass flux are divergenceless, then along every streamline  $\mathbf{B} = \lambda \rho \mathbf{v}$ , where  $\lambda$  is a global constant (Grad, 1960; Spreiter and Rizzi, 1974). (This assumption is very strong and probably does not hold well in the real world, with anisotropic plasma pressures generating plasma instabilities, including ion cyclotron and firehose instabilities (see Quest (1988) for a comprehensive investigation)). We use this assumption to estimate the total incident pressure (summation of magnetosheath thermal and magnetic pressures) along the obstacle under these conditions (using the relation in Section 3.1.3) as

$$P_{T\psi}|_{OB} = k\rho_{\infty}v_{T\infty}^2 \cos^2 \psi + P_{\infty} \sin^2 \psi + \frac{B_{T\infty}^2}{2\mu_0} \left( \frac{\rho_{\psi}v_{\psi}|_{OB}}{\rho_{\infty}v_{T\infty}} \right)^2, \quad (45)$$

where  $\rho_{\psi}|_{OB}$  and  $v_{\psi}|_{OB}$  are given in Table III, for  $\gamma = \frac{5}{3}$ .

When the solar wind magnetic field energy is large enough, however, the Alfvén Mach number and plasma  $\beta$  then are small enough that the ‘switch-on’ shock solution applies. In this case the magnetic field and velocity vectors downstream from the bow shock are still parallel to one another (Kennel and Edmiston, 1988 (neglecting instabilities generated by anisotropies in the plasma)), but the flow is deflected from the subsolar line (the acquired tangential momentum of the downstream flow is compensated by electromagnetic forces within the shock layer). Therefore, the streamline which passes through the subsolar point ( $\alpha_{v-n} = 0^\circ$ ) on the shock surface is no longer the stagnation streamline with zero velocity at the magnetopause. The stagnation streamline at the magnetopause then is one which intersects the bow shock at a non-zero value of  $\alpha_{v-n}$ , and indicates that a simple solution to the Navier–Stokes equation cannot be determined. We are thus unable to solve explicitly for the magnetosheath parameters along the boundary surface. This situation is analogous to that noted by Walters (1964) for IMF directions which are neither aligned with nor perpendicular to the solar wind velocity vector. Walters (1964) predicted that under such conditions, the symmetry axis of the magnetopause will rotate significantly (as much as  $25^\circ$ ) to align itself with the shocked stagnation streamline. It is expected, however, from consideration of the distribution of pressures along the magnetopause (Zhuang et al., 1981) that the symmetry of the entire magnetopause surface will be broken, such that a fit of the dayside magnetopause to an elliptical conic section will result in a rotation of the ellipse symmetry axis which is much less than predicted by Walters (1964) (cf. Russell et al., 1981).

3.3. WITH MAGNETIC FIELD ( $\theta_{B-v} = 90^\circ$ )

We next examine the case for which the upstream magnetic field is perpendicular to the upstream velocity vector. We can determine the thermal pressure, density, and velocity across the bow shock. In addition, an explicit ‘Bernoulli-like’ equation relating the parameters downstream of the bow shock to those at the stagnation position of the obstacle (denoted with the st subscript) can be derived as follows:

$$\frac{1}{2}v_T^2 + \frac{\gamma}{\gamma - 1} \frac{P}{\rho} + \frac{B_T^2}{\mu_0 \rho} = \frac{\gamma}{\gamma - 1} \frac{P_{st}}{\rho_{st}} + \frac{(B_T^2)_{st}}{\mu_0 \rho_{st}}. \quad (46)$$

As before, we also have the adiabatic relation  $P\rho^{-\gamma} = P_{st}\rho_{st}^{-\gamma}$ . However, we cannot decouple the magnetic field from the other components in Equation (46), as we had done earlier for field-aligned flow. Thus, we do not know how the energy is partitioned between the kinetic, thermal, and magnetic components. In addition, along the obstacle the flow is aligned with the draped magnetic field in one direction (along the  $z$ -direction, using the scenario of Figure 3), while the flow is perpendicular to the magnetic field along the orthogonal direction (the  $y$ -axis in Figure 3). The division of pressure between kinetic, thermal, and magnetic pressures appears to be due to additional processes occurring in the flow and is not simply imposed by the (fast) bow shock wave. The most comprehensive and rigorous treatment to date of the flow properties near the magnetopause for an upstream magnetic field which is perpendicular to the upstream flow velocity is the approximate numerical solution of Zwan and Wolf (1976). The Zwan and Wolf model predicts that shocked solar wind plasma is squeezed out along the magnetic field lines, as the plasma is convected towards the magnetopause. This process creates a ‘depletion layer’ close to the magnetopause; a region of depressed plasma density and enhanced magnetic field (assuming no field line merging). This model has received observational support by Crooker et al. (1979), using IMP 6 observations, as well as support from the numerical simulations of Wu (1992).

In contrast to this model, however, it had been argued by Southwood and Kivelson (1992) from consideration of the fundamental modes of plasma wave theory that the opposite effects should be observed close to the magnetopause; i.e., an increase in plasma density and a decrease in magnetic field.

A proposed reconciliation of these contradictory models has recently been presented by Southwood and Kivelson (1995). This model proposes that as the shocked solar wind plasma approaches the magnetopause along the stagnation streamline, it will pass through a slow mode front, thereby increasing the plasma density and decreasing the magnetic field strength. As the plasma continues to move still closer to the magnetopause, however, it must pass through the region described by Zwan and Wolf; namely a decrease in the observed plasma density and increase in the magnetic field strength. Observations of magnetosheath plasma density enhancements and subsequent decreases closer to the magnetopause have

been reported by Song et al. (1990, 1992), using observations by ISEE 1 and 2. All three of the above scenarios were numerically modeled by Lee et al. (1991). The nature of these waves depends on both plasma  $\beta$  and the direction of the IMF with respect to the magnetospheric field. A complete analytic solution remains to be determined, however.

#### 4. Summary

In this study, we have presented an exact solution to the Rankine–Hugoniot relations over the entire bow shock surface. However, the Rankine–Hugoniot relations themselves are only approximations, since parameters such as the thermal pressure are assumed to be well represented by scalar quantities, rather than by tensors. In addition, the equations are non-relativistic and do not account for the curvature of the shock surface. Nevertheless, it is expected that the explicit solutions given above provide an accurate determination of parameters adjacent to the downstream side of the bow shock as a function of the solar wind conditions. We have also examined the phenomenon of the ‘switch-on’ shock solution in context with the Rankine–Hugoniot relations, and its relation to the shock surface as a whole. We find that the ‘switch-on’ shock solution is contained within the solution represented by Equation (13). However, the ‘switch-on’ part of the solution only occurs for cases of magnetosonic Mach numbers close to unity and small values of plasma  $\beta$ . In addition, the ‘switching-on’ of the downstream magnetic field and velocity components parallel to the shock surface occurs only at a singular point on the shock surface; i.e., where the upstream magnetic field direction is exactly normal to the shock surface.

We have also found that the total velocity downstream of the bow shock can slightly exceed the upstream total velocity when the IMF is not perfectly aligned with or perfectly perpendicular to the upstream velocity vector. This is due solely to the frame of reference. In the NIF of reference, the downstream-to-upstream total velocity ratio does not exceed unity anywhere on the shock surface.

Although we understand analytically how the parameters downstream of the bow shock are determined from the upstream parameters, this does not give us any information as to the shock shape or its position from the obstacle. With the use of Bernoulli’s equation and the condition of adiabatic flow we are able to determine the parameters at the stagnation position. However, even with these equations, the spatial gradient from the shock to the obstacle of the changes in pressure, density, or velocity are not known. Thus, without any spatial scales, we are unable to determine the shock standoff position or shape with respect to the obstacle. In hydrodynamics, earlier studies have treated this problem by estimating the form of the stream functions (and related parameters such as vorticity). However, no exact analytic solution has yet been obtained, even for a shock wave in front of a sphere in a purely hydrodynamic flow. Nevertheless, there have been attempts to use the

hydrodynamic results from theory and experiment to develop approximate functions of the distance from the magnetopause to the bow shock along the stagnation streamline (Spreiter et al., 1966; Farris and Russell, 1994; Cairns and Grabbe, 1994; Russell and Petrinec, 1996; Grabbe, 1996). In addition, there are several MHD computational models of the magnetosphere which have been developed (Ogino et al., 1992; Voigt and Wolf, 1988; and others), and could be used to study the shock shape and position and to compare with satellite observations.

We have examined the Newtonian approximation along the surface of an obstacle. Several functions for the pressure relation along the obstacle have been examined in the hydrodynamic situation, and it is found that the best choice of the pressure balance relation, especially for boundaries which are themselves defined via pressure balance, is  $P_{T\psi}|_{OB} = k\rho_\infty v_{T\infty}^2 \cos^2 \psi + P_\infty \sin^2 \psi$ . Other relations which are commonly found in the literature are often useful for their simplicity, but fail either as  $\psi$  approaches  $90^\circ$ , and/or when the upstream sonic Mach number is small (but larger than unity).

We have also examined the Newtonian approximation for specific orientations of the IMF with respect to the upstream velocity vector. When the magnetic field is aligned with the upstream velocity, the pressure exterior to the obstacle can be determined as  $P_{T\psi}|_{OB} = k\rho_\infty v_{T\infty}^2 \cos^2 \psi + P_\infty \sin^2 \psi + B_{T\infty}^2/2\mu_0$  (except when the ‘switch-on’ shock solution is appropriate; then the stagnation streamline no longer coincides with the subsolar streamline, and an exact analytic solution is not yet known).

For general values of  $\theta_{B-v}$ , we have not solved explicitly for the above parameters, because the Navier–Stokes equation (which is an integral equation, but under special circumstances can be reduced to Bernoulli’s equation) cannot be analytically integrated. In addition, the stagnation streamline does not coincide with the subsolar streamline when the IMF and upstream velocity vectors are neither aligned with nor perpendicular to one another. Thus, the total pressure along the obstacle is not exactly known, and only approximate solutions (like those used in the literature) are the best that can be done at present.

Thus, there are several areas for which future efforts at understanding the physics of the magnetosheath region should be directed. The change in parameters across the bow shock are understood analytically; however, analytic and exact functions of the shape and size of the bow shock in relation to the obstacle in an MHD fluid are not yet known. In addition, the properties of the plasma along the obstacle are only known for perfectly aligned flow, when  $M_A^2 > (1 + \gamma(1 - \beta))/(\gamma - 1)$  and  $\beta > 2/\gamma$ . For other orientations of the IMF with respect to the upstream velocity, only rough approximations are used. Lastly, analytic functions of the parameters throughout the entire magnetosheath region would be highly useful but are presently lacking.

### Acknowledgements

One of the authors (S.M.P.) thanks R. A. Wolf, M. Hoshino, and T. K. Nakamura for useful discussions. S.M.P. was supported by a Center of Excellence fellowship at the Institute of Space and Astronautical Science. The work at UCLA was supported by the National Aeronautics and Space Administration under research grant NAGW-3477.

### References

- Beard, D. B.: 1960, 'The Interaction of the Terrestrial Magnetic Field With the Solar Corpuscular Radiation', *J. Geophys. Res.* **65**, 3559–3568.
- Burgess, D.: 1989, 'Cyclic Behavior at Quasi-Parallel Collisionless Shocks', *Geophys. Res. Letters* **16**, 345–348.
- Busemann, A.: 1933, 'Flüssigkeits und Gasbewegung', in *Handwörterbuch der Naturwissenschaften*, Vol. IV, 2nd ed., Gustav Fischer, Jena, p. 244.
- Cairns, I. H. and Grabbe, C. L.: 1994, 'Towards an MHD Theory for the Standoff Distance of Earth's Bow Shock', *Geophys. Res. Letters* **21**, 2781–2784.
- Cairns, I. H. and Lyon, J. G.: 1995, 'MHD Simulations of Earth's Bow Shock at Low Mach Numbers: Standoff Distances', *J. Geophys. Res.* **100**, 17 173–17 180.
- Coroniti, F. V. and Kennel, C. F.: 1972, 'Changes in Magnetospheric Configuration During the Substorm Growth Phase', *J. Geophys. Res.* **77**, 3361–3370.
- Crooker, N. U., Eastman, T. E., and Stiles, G. S.: 1979, 'Observations of Plasma Depletion in the Magnetosheath at the Dayside Magnetopause', *J. Geophys. Res.* **84**, 869–874.
- Daskin, W. and Feldman, L.: 1958, 'The Characteristics of Two-Dimensional Sails in Hypersonic Flow', *J. Aerospace Sci.* **25**, 53–55.
- Dungey, J. W.: 1958, *Cosmic Electrodynamics*, Cambridge University Press, Cambridge, 183 p.
- Dungey, J. W.: 1961, 'The Steady State of the Chapman-Ferraro Problem in Two Dimensions', *J. Geophys. Res.* **66**, 1043–1047.
- Fairfield, D. H.: 1971, 'Average and Unusual Locations of the Earth's Magnetopause and Bow Shock', *J. Geophys. Res.* **76**, 6700–6716.
- Farris, M. H. and Russell, C. T.: 1994, 'Determining the Standoff Distance of the Bow Shock: Mach Number Dependence and Use of Models', *J. Geophys. Res.* **99**, 17 681–17 689.
- Farris, M. H., Petrinec, S. M., and Russell, C. T.: 1991, 'The Thickness of the Magnetosheath: Constraints on the Polytopic Index', *Geophys. Res. Letters* **18**, 1821–1824.
- Ferraro, V. C. A.: 1952, 'On the Theory of the First Phase of a Geomagnetic Storm: A New Illustrative Calculation Based on an Idealized (Plane Not Cylindrical) Model Field Distribution', *J. Geophys. Res.* **57**, 15–49.
- Formisano, V.: 1979, 'Orientations and Shape of the Earth's Bow Shock in Three Dimensions', *Planetary Space Sci.* **27**, 1151–1161.
- Freeman, M. P., Freeman, N. C., and Farrugia, C. J.: 1995, 'A Linear Perturbation Analysis of Magnetopause Motion in the Newton–Busemann Limit', *Ann. Geophys.* **13**, 907–918.
- Grabbe, C. L.: 1996, 'MHD Theory of Earth's Magnetosheath for an Axisymmetric Model', *Geophys. Res. Letters* **23**, 777–780.
- Grabbe, C. L. and Cairns, I. H.: 1995, 'Analytic MHD Theory for Earth's Bow Shock at Low Mach Numbers', *J. Geophys. Res.* **100**, 19 941–19 949.
- Grad, H.: 1960, 'Reducible Problems in Magneto-fluid Dynamic Steady Flows', *Rev. Mod. Phys.* **32**, 830–847.
- Hayes, W. D.: 1955, 'Some Aspects of Hypersonic Flow', The Ramo-Wooldridge Corp.
- Hida, K.: 1953, 'An Approximate Study on the Detached Shock Wave in Front of a Circular Cylinder and a Sphere', *J. Phys. Soc. Japan* **8**, 740–745.
- Howe H. C., Jr. and Binsack, H. H.: 1972, 'Explorer 33 and 35 Plasma Observations of Magnetosheath Flow', *J. Geophys. Res.* **77**, 3334–3344.

- Hudson, P. D.: 1970, 'Discontinuities in an Anisotropic Plasma and Their Identification in the Solar Wind', *Planetary Space Sci.* **18**, 1611–1622.
- Hurley, J.: 1961, 'Interaction Between the Solar Wind and the Geomagnetic Field', New York University College of Engineering Report.
- Kawamura, T.: 1950, *On the Detached Shock Wave in Front of a Body Moving at Speeds Greater Than That of Sound*, University of Kyoto, College of Science, Memoirs, Ser. A, Vol. XXVI, No. 3, p. 207–232.
- Kellogg, P. J.: 1962, 'Flow of Plasma Around the Earth', *J. Geophys. Res.* **67**, 3805–3811.
- Kennel, C. F. and Edmiston, J. P.: 1988, 'Switch-On Shocks', *J. Geophys. Res.* **93**, 11 363–11 373.
- Laitone, E. V. and Pardee, O. O'M.: 1947, *Location of Detached Shock Wave in Front of a Body Moving at Supersonic Speeds*, NACA RM A7B10.
- Landau, L. O. and Lifshitz, E. M.: 1959, *Fluid Mechanics*, Pergamon, New York.
- Lee, L. C., Yan, M., and Hawkins, J. G.: 1991, 'A Study of Slow-Mode Structures in the Dayside Magnetosheath', *Geophys. Res. Letters* **18**, 381–384.
- Lepping, R. P. and Argentiero, P. D.: 1971, 'Single Spacecraft Method of Estimating Shock Normals', *J. Geophys. Res.* **76**, 4349–4359.
- Linnell, R. D.: 1958, 'Hypersonic Flow Around a Sphere', *J. Aerospace Sci.* **25**, 65–66.
- Lomax, H. and Inouye, M.: 1964, *Numerical Analysis of Flow Properties About Blunt Bodies Moving at Supersonic Speeds in an Equilibrium Gas*, NASA Tech. Rep. R-204, p. 1–78.
- Mead, G. D.: 1966, in R. J. Mackin, Jr. and M. Neugebauer (eds.), 'The Shape of the Magnetosphere and the Distortion of the Geomagnetic Field', *The Solar Wind*, Pergamon Press, New York, p. 337.
- Mead, G. D. and Beard, D. B.: 1964, 'Shape of the Geomagnetic Field Solar Wind Boundary', *J. Geophys. Res.* **69**, 1169–1179.
- Nagamatsu, H. T.: 1949, *Theoretical Investigations of Detached Shock Waves*, GALCIT Publ.
- Ogino, T., Walker, R. J., and Ashour-Abdalla, M.: 1992, 'A Global Magnetohydrodynamic Simulation of the Magnetosheath and Magnetosphere When the Interplanetary Magnetic Field is Northward', *IEEE Trans. Plasma Sci.* **20**, 817–828.
- Olson, W. P.: 1969, 'The Shape of the Tilted Magnetopause', *J. Geophys. Res.* **74**, 5642–5651.
- Onsager, T. G., Winske, D., and Thomsen, M. F.: 1991a, 'Interaction of a Finite-Length Ion Beam With a Background Plasma: Reflected Ions at the Quasi-Parallel Shock', *J. Geophys. Res.* **96**, 1775–1788.
- Onsager, T. G., Winske, D., and Thomsen, M. F.: 1991b, 'Ion Interaction Simulations of Quasi-Parallel Shock Re-formation', *J. Geophys. Res.* **96**, 21 183–21 194.
- Parker, E. N.: 1961, 'The Solar Wind', in W. Liller (ed.), *Space Astrophysics*, pp. 157–170, McGraw-Hill Book Co., New York, 272 pp.
- Parks, G. K.: 1991, *Physics of Space Plasmas*, Addison-Wesley, Redwood City, CA, 538 pp.
- Peredo, M. J., Slavin, A., Mazur, E., and Curtis, S. A.: 1995, 'Three-Dimensional Position and Shape of the Bow Shock and Their Variation With Alfvénic, Sonic and Magnetosonic Mach Numbers and Interplanetary Magnetic Field Orientation', *J. Geophys. Res.* **100**, 7907–7916.
- Petrinec, S. M. and Russell, C. T.: 1993, 'An Empirical Model of the Size and Shape of the Near-Earth Magnetotail', *Geophys. Res. Letters* **20**, 2695–2698.
- Petrinec, S. M. and Russell, C. T.: 1996, 'The Near-Earth Magnetotail Shape and Size as Determined From the Magnetopause Flaring Angle', *J. Geophys. Res.* **101**, 137–152.
- Piddington, J. H.: 1960, 'Geomagnetic Storm Theory', *J. Geophys. Res.* **65**, 93–106.
- Quest, K. B.: 1988, 'Theory and Simulation of Collisionless Parallel Shocks', *J. Geophys. Res.* **93**, 9649–9680.
- Russell, C. T. and Petrinec, S. M.: 1996, 'Comments on "Towards an MHD Theory for the Standoff Distance of Earth's Bow Shock" by I. H. Cairns and C. L. Grabbe', *Geophys. Res. Letters* **23**, 309–310.
- Russell, C. T., Zhuang, H. C., Walker, R. J., and Crooker, N. C.: 1981, 'A Note on the Location of the Stagnation Point in the Magnetosheath Flow', *Geophys. Res. Letters* **8**, 984–986.
- Scholer, M. and Burgess, D.: 1992, 'The Role of Upstream Waves in Supercritical, Quasi-Parallel Shock Re-formation', *J. Geophys. Res.* **97**, 8319–8326.

- Scholer, M., Fujimoto, M., and Kucharek, H.: 1993, 'Two-Dimensional Simulations of Supercritical Quasi-Parallel Shocks: Upstream Waves, Downstream Waves, and Shock Re-formation', *J. Geophys. Res.* **98**, 18 971–18 984.
- Seiff, A.: 1962, *Recent Information on Hypersonic Flow Fields*, NASA SP-24, pp. 19–32.
- Sibeck, D. G.: 1995, 'Demarcating the Magnetopause Boundary', *Rev. Geophys. Suppl.* **33**, 651–655.
- Sibeck, D. G., Siscoe, G. L., Slavin, J. A., Smith, E. J., Tsurutani, B. T., and Lepping, R. P.: 1985, 'The Distant Magnetotail's Response to a Strong IMF By Twisting, Flattening, and Field Line Bending', *J. Geophys. Res.* **90**, 4011–4019.
- Sibeck, D. G., Lopez, R. E., and Roelof, E. C.: 1991, 'Solar Wind Control of the Magnetopause Shape, Location, and Motion', *J. Geophys. Res.* **96**, 5489–5495.
- Slavin, J. A., Smith, E. J., Sibeck, D. G., Baker, D. N., Zwickl, R. D., and Akasofu, S.-I.: 1985, 'An ISEE 3 Study of Average and Substorm Conditions in the Distant Magnetotail', *J. Geophys. Res.* **90**, 10 875–10 895.
- Song, P., Russell, C. T., Gosling, J. T., Thomsen, M. F., and Elphic, R. C.: 1990, 'Observations of the Density Profile in the Magnetosheath Near the Stagnation Streamline', *Geophys. Res. Letters* **17**, 2035–2038.
- Song, P., Russell, C. T., and Thomsen, M. F.: 1992, 'Slow Mode Transition in the Frontside Magnetosheath', *J. Geophys. Res.* **97**, 8295–8305.
- Southwood, D. J. and Kivelson, M. G.: 1992, 'On the Form of the Flow in the Magnetosheath', *J. Geophys. Res.* **97**, 2873–2879.
- Southwood, D. J. and Kivelson, M. G.: 1995, 'Magnetosheath Flow Near the Subsolar Magnetopause: Zwan–Wolf and Southwood–Kivelson Theories Reconciled', *Geophys. Res. Letters* **22**, 3275–3278.
- Spitzer, L., Jr.: 1956, *Physics of Fully Ionized Gases*, Interscience Publ., New York.
- Spreiter, J. R. and Alksne, A. Y.: 1968, 'Comparison of Theoretical Predictions of the Flow and Magnetic Field Exterior to the Magnetosphere with Observations of Pioneer 6', *Planetary Space Sci.* **16**, 971–979.
- Spreiter, J. R. and Alksne, A. Y.: 1969, 'Effect of Neutral Sheet Currents on the Shape and Magnetic Field of the Magnetosphere Tail', *Planetary Space Sci.* **17**, 233–246.
- Spreiter, J. R. and Briggs, B. R.: 1961, *Theoretical Determination of the Form of the Hollow Produced in a Solar Corpuscular Stream by the Interaction With the Magnetic Dipole Field of the Earth*, NASA TR R-120.
- Spreiter, J. R. and Briggs, B. R.: 1962, 'Theoretical Determination of the Form of the Boundary of the Corpuscular Stream Produced by Interaction with the Magnetic Dipole Field of the Earth', *J. Geophys. Res.* **67**, 37–51.
- Spreiter, J. R. and Rizzi, A. W.: 1974, 'Aligned Magnetohydrodynamic Solution for Solar Wind Flow Past the Earth's Magnetosphere', *Acta Astrophys.* **1**, 15–35.
- Spreiter, J. R. and Stahara, S. S.: 1985, in B. T. Tsurutani and R. G. Stone (eds.), 'Magnetohydrodynamic and Gasdynamic Theories for Planetary Bow Waves', *Collisionless Shocks in the Heliosphere: Review of Current Research*, AGU Monograph, Vol. 35, pp. 85–107.
- Spreiter, J. R. and Stahara, S. S.: 1995, 'The Location of Planetary Bow Shocks: A Critical Overview of Theory and Observations', *Adv. Space Res.* **15** (8/9), 433–449.
- Spreiter, J. R. and Jones, W. P.: 1963, 'On the Effect of a Weak Interplanetary Magnetic Field on the Interaction Between the Solar Wind and the Geomagnetic Field', *J. Geophys. Res.* **68**, 3555–3564.
- Spreiter, J. R., Summers, A. L., and Alksne, A. Y.: 1966, 'Hydromagnetic Flow Around the Magnetosphere', *Planetary Space Sci.* **14**, 223–253.
- Szabo, A.: 1994, 'An Improved Solution to the "Rankine–Hugoniot" Problem', *J. Geophys. Res.* **99**, 14 737–14 746.
- Thomas, V. A., Winske, D., and Omid, N.: 1990, 'Re-forming Supercritical Quasi-Parallel Shocks, 1. One- and Two-dimensional Simulations', *J. Geophys. Res.* **95**, 18 809–18 820.
- Unti, T. and Atkinson, G.: 1968, 'Two-Dimensional Chapman–Ferraro Problem with Neutral Sheet, 1. The Boundary', *J. Geophys. Res.* **73**, 7319–7327.
- Van Dyke, M. D. and Gordon, H. D.: 1959, *Supersonic Flow Past a Family of Blunt Axisymmetric Bodies*, NASA Tech. Rep. R-1, pp. 1–25.

- Viñas, A. F. and Scudder, J. D.: 1986, 'Fast and Optimal Solution to the "Rankine–Hugoniot Problem"', *J. Geophys. Res.* **91**, 39–58.
- Voigt, G.-H. and Wolf, R. A.: 1988, 'Quasi-Static Magnetospheric MHD Processes and the 'Ground State' of the Magnetosphere', *Rev. Geophys.* **26**, 823–843.
- Walters, G. K.: 1964, 'Effect of Oblique Interplanetary Magnetic Field on Shape and Behavior of the Magnetosphere', *J. Geophys. Res.* **69**, 1769–1783.
- Winske, D., Omid, N., Quest, K. B., and Thomas, V. A.: 1990, 'Re-forming Supercritical Quasi-Parallel Shocks, 2. Mechanism for Wave Generation and Front Re-formation', *J. Geophys. Res.* **95**, 18 821–18 832.
- Wu, C. C.: 1992, 'MHD Flow Past an Obstacle: Large-Scale Flow in the Magnetosheath', *Geophys. Res. Letters* **19**, 87–90.
- Zhang, T.-L., Luhmann, J. G., and Russell, C. T.: 1991, 'The Magnetic Barrier at Venus', *J. Geophys. Res.* **96**, 11 145–11 153.
- Zhang, T.-L., Schwingenschuh, K., Russell, C. T., Luhmann, J. G., Rosenbauer, H., Verigin, M. I., and Kotova, G.: 1994, 'The Flaring of the Martian Magnetotail Observed by the Phobos 2 Spacecraft', *Geophys. Res. Letters* **21**, 1121–1124.
- Zhang, T.-L., Schwingenschuh, K., Petrinec, S. M., Russell, C. T., Luhmann, J. G., Rosenbauer, H., Verigin, M. I., and Kotova, G.: 1995, 'Studies of the Draping and Flaring Angles of the Mars and Earth Magnetotails', *Adv. Space Res.* **16** (4), 99–103.
- Zhigulev, V. N. and Romishevskii, E. A.: 1959, 'Concerning the Interaction of Currents Flowing in a Conducting Medium With the Earth's Magnetic Field', *Doklady Akad. Nauk SSSR* **127**, 1001–1004 (English translation: 1960, *Soviet Phys. Doklady* **4**, 859–862).
- Zhuang, H. C., Russell, C. T., and Walker, R. J.: 1981, 'The Influence of Interplanetary Magnetic Field and Thermal Pressure on the Position and Shape of the Magnetopause', *J. Geophys. Res.* **86**, 10 009–10 021.
- Zhuang, H. C. and Russell, C. T.: 1981, 'An Analytic Treatment of the Structure of the Bow Shock and Magnetosheath', *J. Geophys. Res.* **86**, 2191–2205.
- Zwan, B. J. and Wolf, R. A.: 1976, 'Depletion of Solar Wind Near a Planetary Boundary', *J. Geophys. Res.* **81**, 1636–1648.